molecular pharmaceutics

pubs.acs.org/molecularpharmaceutics

Article

Topical Administration of Mucoadhesive Liposomes–Epoetin-β for Targeting the Ocular Posterior Segment

Sarvenaz Pakian, Mohammad reza Nabid,* Leila Satarian, Hamid Sadeghi Abandansari,* and Ahmad Mirkani

Cite This: *Mol. Pharmaceutics* 2025, 22, 2287−2305

Read Online

ACCESS | Metrics & More | Article Recommendations | Supporting Information

ABSTRACT: Delivering drugs to the posterior eye segment is a complex task, particularly for treating retinal diseases. Neuroprotective approaches to maintain neuronal integrity have garnered significant attention in recent research. Here, we developed a mucoadhesive nanoparticulate system based on thiolated hyaluronic acid-modified cationic liposomes (HA-SH@liposomes) for topical administration. To fabricate these liposomes, we utilized microfluidic technology with a toroidal mixer to ensure consistent size and stability. Cationic liposomes were prepared by using the microfluidic method, and Epoetin-β (EPOβ), a neuroprotective agent, was loaded into the liposomes. Following this, HA-SH was conjugated to the EPOβ/HA-SH@liposomes using a postmicrofluidics conjugation method, wherein HA-SH was added dropwise to facilitate electrostatic interactions between the cationic liposomes and the anionic polymer. The resulting liposomes exhibited a mean size of 144 ± 1.3 nm and a polydispersity index (PDI) of 0.09 ± 0.01, indicating their uniformity. We evaluated the biocompatibility of the EPOβ/HA-SH@liposomes in vitro using live/dead and MTS assays on the RGC-5 cell line, demonstrating no notable cytotoxicity compared to the controls. To assess the in vivo performance, we conducted extensive ophthalmological examinations in C57/BL6 mice, including immunofluorescence staining to track the distribution of EPOβ and EPOβ/HA-SH@liposomes within the eyeball. Additionally, we quantified EPOβ levels in the retina using an enzyme-linked immunosorbent assay (ELISA) kit after the topical application of free EPOβ and the EPOβ/HA-SH@liposome formulation. The immunofluorescence staining revealed efficient delivery of EPOβ into the retina and choroid via the transcorneal route when administered as EPOβ/HA-SH@liposomes. ELISA results showed that the liposomal formulation achieved approximately 1.9× greater penetration efficiency than free EPOβ. Furthermore, optokinetic response (OKR) assays indicated that animals treated with EPOβ/HA-SH@liposomes exhibited slightly improved visual acuity compared with those treated with free EPOβ, though the difference was not statistically significant. In conclusion, the topical ocular administration of EPOβ/HA-SH@liposomes facilitated the efficient delivery of EPOβ to the retina, promoting retinal recovery and confirming its neuroprotective properties. This preclinical study provides a foundation for innovative strategies in the topical delivery of neuroprotective agents in ocular therapy.

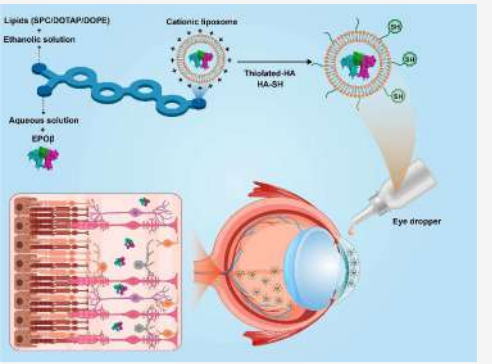

KEYWORDS: *Epoetin-β (EPOβ), Erythropoietin, Cationic liposomes, Microfluidics, Optic nerve crush (ONC), Mucoadhesion, Hyaluronic acid (HA)*

INTRODUCTION

Posterior ocular drug delivery faces significant challenges in achieving an optimum drug concentration due to the unique protective mechanisms of the eye. Creating a drug delivery system to achieve therapeutic concentrations at the intended site necessitates thoroughly comprehending the static and dynamic barriers within the eye.[1,2] The posterior segment of the eye comprises the back two-thirds of the eye, including the vitreous humor, the retina, the choroid, and the optic nerve.[3] Neurodegenerative ocular diseases such as glaucoma, age-related macular degeneration (AMD), diabetic retinopathy (DR), and diabetic macular edema (DME) are major causes of irreversible blindness worldwide, all affecting the posterior segment of the eye.[4]

Erythropoietin (EPO), a glycoprotein primarily produced in the adult kidneys and fetal liver, plays a key hematopoietic role by promoting erythrocyte production in the bone marrow.[5] Interestingly, new EPO-secreting sites, such as the brain[6] and the retina,[7] have been identified, expressing EPO receptors.[8,9] Recent research has highlighted the tissue-protective properties of EPO in the brain, heart, inner ear, and retina.[10]

Received: January 18, 2025
Revised: February 27, 2025
Accepted: March 4, 2025
Published: March 18, 2025

https://doi.org/10.1021/acs.molpharmaceut.5c00079
Mol. Pharmaceutics 2025, 22, 2287−2305

Furthermore, the subconjunctival administration of EPO has been investigated as an alternative delivery method targeting the posterior ocular segment, yielding encouraging results.[11,12] For instance, in glaucomatous rats, the subconjunctival delivery of epoetin-β (EPOβ), a recombinant version of EPO, improved retinal health compared to untreated animals.[13]

EPOβ has demonstrated significant neuroprotective and neuroregenerative effects across various models of neurodegenerative diseases, both ocular and nonocular. This is explained by its capacity to reduce apoptosis, inflammation, oxidative stress, and excitotoxicity[14,15] while promoting progenitor cell proliferation.[5] Consequently, EPOβ appears to be a promising drug for preventing retinal ganglion cells (RGC) death.[16,17]

Current methods for treating diseases of the posterior ocular segment include intravitreal, systemic, and subconjunctival drug administration.[18] Intravitreal injections, while effective, are invasive and carry potential side effects, such as intraocular hemorrhage, endophthalmitis, cataracts, and retinal toxicity. Systemic administration requires high drug doses, which can lead to serious side effects.[3] Subconjunctival administration is less invasive and has fewer side effects, but it still requires patient cooperation and/or light sedation.[19] Therefore, there is a critical need for noninvasive drug delivery systems that ensure effective treatment while minimizing risks and improving patient comfort. Topical eye drops represent the most common noninvasive method for ocular drug delivery.[20] However, the bioavailability of conventional eye drops is notoriously low, with only 1−5% of the drug applied to the ocular surface penetrating the inner eye.[21] The corneal epithelium's lipophilic nature hinders the penetration of hydrophilic drugs, and the rapid clearance of the drug due to precorneal barriers further limits its effectiveness.[22] Large macromolecules like EPOβ, CRISPR-Cas9, and siRNA face additional challenges in passive uptake and crossing ocular barriers, impeding their therapeutic delivery to the retina.[23,24]

Nanoparticle-based drug delivery systems have significantly improved the treatment of posterior eye diseases through topical administration.[25] Ideal formulations should enhance retention on the ocular surface, improve drug permeability, and ensure targeted drug delivery.[26,27] Mucoadhesive nanoparticles are cutting-edge systems that fulfill these requirements by protecting the drug and enhancing its permeation through biological barriers at the same time.[28] In 2022, Beatriz Silva and colleagues demonstrated that chitosan-hyaluronic acid nanoparticles (CS/HA) effectively delivered EPOβ to the posterior segment of the eye through subconjunctival administration, with EPOβ detected in the retina for up to 21 days postdelivery.[29] Further studies in 2023 confirmed the safety and efficacy of these nanoparticles for topical delivery of EPOβ to the retina.[30]

In addition to mucoadhesive nanoparticles, colloidal drug delivery systems such as liposomes have also shown promise. By interacting with the ocular mucosa, colloidal particles can increase the permeability of the cornea and conjunctiva.[31] Liposomes are spherical vesicles of phospholipid bilayers that encapsulate an aqueous core, and their modification with mucoadhesive polymers, like hyaluronic acid, can enhance their retention time on the ocular surface.[32,33] Over recent decades, liposomal formulations have been shown to effectively deliver drugs to the eye, and this strategy holds considerable potential for improving the delivery of therapeutic agents.[34,35]

In this study, we developed a mucoadhesive nanoparticulate system consisting of EPOβ-loaded cationic liposomes coated with thiolated hyaluronic acid (EPOβ/HA-SH@liposomes). The liposomal formulation of EPOβ was prepared using a microfluidic method, a robust technology that allows precise control over fluid flow, mixing, and droplet formation. This approach is crucial for producing highly reproducible and scalable formulations, ensuring consistency in the final product. By enabling the uniform mixing of lipids and aqueous solutions at a microscale, this method ensures the formation of liposomes with precisely controlled size, high encapsulation efficiency, and enhanced stability.

We investigated several key properties of the system including stability, drug loading capacity (DL%), encapsulation efficiency (EE%), zeta potential, and particle size. Mucoadhesion studies of the liposomes, HA@liposomes, and HA-SH@liposomes were performed using viscosity and zeta potential measurements. To evaluate the HA-specific CD44 receptor interaction, the uptake of these vectors was assessed using absorbance measurements.

The ocular biocompatibility of the EPOβ/HA-SH@liposomes was assessed in vitro using live/dead and MTS assays with the mouse retinal ganglion cell line (RGC-5). The biological effects of the nanoformulation were further evaluated in vivo through immunofluorescence following topical ocular administration. EPOβ levels in mice after the topical administration of EPOβ, HA-SH@liposomes, and EPOβ/HA-SH@liposomes were measured by using an enzyme-linked immunosorbent assay (ELISA). Additionally, a visual behavioral assessment was conducted by using optokinetic response (OKR) assays to evaluate the efficacy of topical formulations.

2. MATERIALS AND METHODS

2.1. Materials. Hyaluronic acid (HA, sodium salt, cosmetic grade, MW = 10000 Da) was obtained from Bloomage Freda Biopharm Corporation (Shandong, China). 1,2-Dioleoyl-*sn*-glycero-3-phospho ethanol amine (DOPE), L-α-phosphatidylcholine (SPC, 95%), and 1,2-dioleoyl-3-trimethylammonium-propane (DOTAP) were purchased from Lipoid Co. (Germany). Cinnapoietin 10000 UI/mL (erythropoietin-β) was purchased from Cinnagen Company (Tehran, Iran). *N*-Hydroxysuccinimide (NHS, 99%), 5,5′-dithiobis-(2-nitrobenzoic acid) (DTNB, 99%), cysteamine hydrochloride (CSA·HCl, 99%), 3-(4,5-dimethylthiazol-2-yl)-5-(3-carboxymethoxyphenyl)-2-(4-sulfophenyl)-2*H*-tetrazolium (MTS), 1-ethyl-3-(3-dimethyl aminopropyl) carbodiimide hydrochloride (EDCI, 99%), and anti-erythropoietin produced in rabbit (IgG fraction of antiserum) were purchased from Sigma-Aldrich Co (Supporting Table 1). Additionally, dried mucin from pig stomach type II (Sigma-Aldrich, Saint Louis, MI, USA) was employed for the mucoadhesive investigations. In every step of analysis, ultrapure water was utilized, and additional chemicals of analytical grade were employed.

2.2. Chemical Characterization and Instrumentation. The particle size, polydispersity index (PDI), apparent zeta potential, and surface charge of the samples were measured using dynamic light scattering (DLS) with a HORIBA DLS-7100 instrument (Japan). Utilizing a transmission electron microscope (TEM) with an accelerating voltage of 100 kV, a Philips EM 208S system was used to study the morphology of the nanoparticles. UV−visible spectra were obtained by using a Shimadzu UV-2400 spectrophotometer. Using a Tescan Vegan

https://doi.org/10.1021/acs.molpharmaceut.5c00079
Mol. Pharmaceutics 2025, 22, 2287−2305

system, field emission scanning electron microscopy (FE-SEM) was used to investigate the microstructure. The BRUKER DRX-300 AVANCE spectrometer was used to record proton nuclear magnetic resonance (^{1}H NMR) spectra. In this study, a cooling centrifuge (Sigma 3−18KS; Sigma, Aachen, Germany) was used. Ultracentrifugation was performed with a Beckman J2−21 M centrifuge and a JA-14 rotor. Images were captured using an IX71 fluorescence and confocal microscope (Zeiss LSM 800).

2.3. Synthesis of Thiolated Hyaluronic Acid (HA-SH). The following method was used to synthesize the HA-SH.[36] The first step involved completely dissolving 400 mg of HA and 230 mg (2 mmol) of NHS in 80 mL of deionized water at room temperature while mixing. After adding 383 mg (2 mmol) of EDCI to the mixture, mixing it thoroughly, and allowing it to react for 2 h, the carboxylic group of HA was subsequently activated. Subsequently, 10 mL of deionized water was used to dissolve 114 mg (1 mmol) of CSA·HCl, which was then added to the mixture. 1.0 M NaOH or 1.0 M HCl was added to the solution as needed to keep its pH at 4.75 throughout the procedure. After the mixture was agitated for a full day, it was moved to the dialysis tube (cut off at 3500 Da) and vigorously dialyzed against a diluted HCl solution (pH 3.5) containing 100 mM NaCl for 48 h. Eventually, lyophilizing the acidified solution created the HA-SH solid. Using a ^{1}H NMR spectrum, the molecular structures of HA-SH and HA were identified.

2.4. Preparation of Cationic Liposomes (SPC/DOPE/DOTAP). Positively charged liposomes were synthesized using a toroidal micromixer and the desktop NanoSynthesizer equipment (INSIGHT, NanoSynthes Co.), which facilitated rapid mixing of formulation solutions within a microfluidic cartridge. The cartridge, equipped with two inlets, introduced lipid mixtures dissolved in ethanol (EtOH) into one inlet and PBS into the other. The flow rate ratio (FRR: 1:5, EtOH/PBS) and total flow rate (TFR: 10 mL/min) were controlled via the NanoSynthesizer interface. Lipid concentrations were initially set at 20 mM with the lipid ratios SPC/DOTAP/DOPE of 50:25:25, 55:25:20, and 55:30:15 (Table 1). Lipid mixtures in ethanol were combined with the aqueous phase consisting of PBS (10 mM, pH 7.4) with initial EPOβ concentrations of 1000 IU/mL for EPOβ-loaded liposomes. Liposome formulations were collected from the chamber outlet and dialyzed against PBS to remove residual solvent.

Table 1. Mass and Molar Ratios of the Formulations

formulation code	SPC/DOPE/DOTAP mass ratio	SPC/DOPE/DOTAP molar ratio
L1	2.08:1:0.93	50:25:25
L2	3.06:1.33:1	55:25:20
L3	4.44:1.77:1	55:30:15

Optimizing conditions such as FRR and lipid ratios was critical to achieving the smallest particle size and lowest PDI. Variations in FRR were systematically tested for each lipid ratio to evaluate their effects on the liposome diameter, PDI, and zeta potential.

2.5. Preparation of HA-SH@liposomes. The cationic EPOβ-liposome suspension was subjected to the dropwise addition of an anionic HA-SH aqueous solution (0.01−0.1 mg/mL) at a 4:1 volume ratio of liposome to polymer under magnetic stirring at 500 rpm for 60 min. The HA-SH concentration was adjusted to 0.05% (w/v). After 30 min of ultracentrifugation at 20 000 × g at 4 °C, the pellet was washed once with distilled water to remove excess polyelectrolytes and resuspended in sterile PBS.[37] The presence of HA-SH on the liposome surface was determined by using FITC-labeled liposomes. Changes in the maximum absorbance peak of the UV−visible spectrum, measured with a Shimadzu UV-2400 spectrophotometer, were indicative of successful HA-SH coating.[38]

2.6. EPOβ Entrapment Efficiency (EE%) and Drug Loading Content (DL%) by Centrifugal Ultrafiltration Method. The EE% and DL% of the liposomes produced by a microfluidic technique were confirmed by centrifugal ultrafiltration.[39] To put it briefly, centrifugal filter tubes (Vivaspin 20 Ultrafiltration Unit; molecular weight (MW) cutoff OF 100 kDa) were used to centrifuge the EPOβ loaded liposomes for 30 min at 8000 rpm at 4 °C. The liposomes were removed from the aqueous phase, and the free EPOβ was measured in the supernatant using a MicroBCA Kit Assay (Pierce, UK) and compared to the total amount supplied to the nanoformulation. The following formulas were used to determine the EE% and DL%.[40,41] (*It is important to note that this method assumes 100% mass balance, meaning that all the EPOβ is either encapsulated within the liposomes or remains in the free form.*)

$$\text{EE\%} = \frac{[\text{Total protein}] - [\text{Free Protein}]}{[\text{Total protein}]} \times 100 \quad (1)$$

$$\text{DL\%} = \frac{[\text{Total protein}] - [\text{Free Protein}]}{[\text{Mass nanoparticles}]} \times 100 \quad (2)$$

2.7. In Vitro Permeation Study. Glass diffusion cells of Franz type, constructed in-house, were used to evaluate the in vitro permeation of EPOβ from drug-loaded liposomal formulations. The diffusion area of the cells was 1.8 cm^2, and the receptor and donor compartments were separated by a cellulose membrane with a molecular weight cutoff of 50 kDa. Before use, the membrane was soaked in double-distilled water for 12 h and then mounted in the Franz diffusion cell. The donor compartment was loaded with liposomal formulations (EPOβ/HA-SH@liposomes (1000 IU of EPOβ in 5 mL liposomes), EPOβ/liposomes, and free EPOβ), which were dialyzed against a receptor medium consisting of simulated tear fluid (STF: NaCl (0.67 g), $NaHCO_3$ (0.20 g), $CaCl_2{\cdot}2H_2O$ (0.008 g), and purified water to (100 g)).[42] The concentration of EPOβ in all three groups (EPOβ/HA-SH@liposomes, EPOβ/liposomes, and free EPOβ) is 0.00168 mg/mL (1.68 μg/mL). The system was maintained at a constant temperature of 37 °C with a stirring rate of 300 rpm. Samples were collected at predefined time intervals: 1, 2, 4, 6, 8, 24, 48, and 72 h. The incubation medium in all cases was replaced daily. Protein content in the receptor samples was quantified using the MicroBCA Kit Assay (Pierce, UK).

The drug permeation kinetics of EPOβ from the formulations (free EPOβ, EPOβ/liposomes, and EPOβ/HA-SH@liposomes) were analyzed using four kinetic models: zero-order (constant permeation rate), first-order (permeation dependent on drug concentration), Higuchi (diffusion-based permeation), and Korsmeyer−Peppas (mechanistic model for permeation from delivery systems).

2.8. Physicochemical and Structural Characterization of Liposomes. *2.8.1. Particle Size, PDI, Zeta Potential, and Morphology.* At a concentration of 0.2 mM, DLS was used to

https://doi.org/10.1021/acs.molpharmaceut.5c00079
Mol. Pharmaceutics 2025, 22, 2287−2305

assess the liposomes' particle sizes and PDI, while electrophoretic light scattering was employed to determine the zeta potential values. The morphology of the liposomes was analyzed by using TEM and FE-SEM techniques. The TEM method provided insights into the internal structure of the particles, while FE-SEM was utilized to examine the external structure and surface characteristics. For FE-SEM analysis, a drop of the liposomal suspension was applied to a clean mica surface and dried at 30 °C. The sample was then coated with platinum using a Quorum MIRA3 Sputter Coater (Quorum Technologies) and inspected with an FEI Quanta FE-SEM. For TEM analysis, a drop of the sample was placed on a copper grid covered with a carbon film. After approximately 10 s of negative staining with a 2% uranyl acetate solution, the grid was blotted dry and analyzed.

2.8.2. Stability Studies. The stability of the optimized liposomal formulations (HA-SH@liposomes) was assessed in terms of both physical and chemical stability. For physical stability, the formulations were stored at 4 and 37 °C for 4 weeks, with regular measurements of size (Z-average), zeta potential, and PDI to monitor structural integrity, aggregation, and homogeneity over time. In addition to these analyses, we also investigated the drug leakage of the HA-SH@liposomes system at 4 and 37 °C. Drug leakage serves as a critical parameter for assessing the retention and release capabilities of the liposomal system under different storage conditions, providing further insight into its stability and functionality.

For chemical stability, a comparison was made between HA-SH@liposomes and bare liposomes, focusing on their resistance to lipid oxidation. The HA-SH coating, characterized by its higher zeta potential, provided enhanced electrostatic repulsion, preventing vesicle coalescence and reducing oxidation by rejecting transition metals that catalyze such reactions. To ensure an accurate analysis, both formulations were stored at 4 °C immediately after production. DLS measurements, including size (Z-average), zeta potential, and PDI, were recorded alongside chemical stability assessments at regular intervals over the study period (4 weeks at days 1, 7, 14, 21, and 28).

2.9. Mucoadhesion Studies. Measurements of the zeta potential and viscosity were used to assess mucoadhesion. To achieve a 10% (w/w) dispersion at 20−25 °C, the mucin employed in this investigation was hydrated with water while being gently stirred until it completely dissolved. The Ostwald viscometer is used to measure viscosity.

2.9.1. Viscosity. The following formula was used to estimate the eye drop solutions' viscosity characteristics at room temperature using the Ostwald viscometer (Fisher Scientific, Pittsburgh, PA, Hampton, NH, USA):

$$\eta_1 = \eta_2 \cdot \rho_1 t_1 / \rho_2 t_2 \tag{3}$$

In the viscometer, the viscosity coefficients of the solution and water are represented by η_1 and η_2, the densities of the solution and water are represented by ρ_1 and ρ_2, and the flow times of the solution and water are represented by t_1 and t_2, respectively. Each component's viscosity (HA@liposome, HA-SH@liposome, and mucin) was first measured in triplicate, and the average of the results was calculated. Three samples were created to assess the impact of the mucin's interaction with the solutions: (1) 5% (w/w) mucin suspension, (2) mucin suspension + HA@liposomes solution (1:1), and (3) mucin suspension + HA-SH@liposomes solution (1:1). The equation below was used to express mucoadhesion:

$$\Delta(\%) = \frac{[\eta_{muc+HA} - (\eta_{muc} + \eta_{HA})]}{(\eta_{muc} + \eta_{HA})} \times 100 \tag{4}$$

The mucoadhesion index is represented by $\Delta(\%)$, while the dynamic viscosity of the mucin, product, and mucin-containing solution and product are represented by η_{muc}, η_{HA}, and η_{muc+HA}, respectively. The η_{muc+HA} for a mucoadhesive polymer, such as HA, is greater than $(\eta_{muc} + \eta_{HA})$ because of interactions between the polymer and mucin. An indicator of mucoadhesive strength is the mucoadhesive index.[43]

2.9.2. Zeta Potential. The zeta potentials of the mucin mixtures and each solution were also measured to evaluate the mucoadhesion interaction. To check for bubbles that would interfere with the zeta potential measurements, 40 μL of each sample was diluted in 2 mL of filtered pure water before the cell was filled. Every experiment was carried out in triplicate.

2.10. Cell Line and Cell Culture. RGC-5 cells at passage 10 were obtained from the Royan Institute Cell Bank in Tehran, Iran, and cultivated in Dulbecco's Modified Eagle Medium (#31600083, Gibco), which contained 200 mM GlutaMAX (#35050038, Gibco), 10% fetal bovine serum (#10270106, Gibco), and 1 g/L glucose supplemented with 3.7 g/L sodium bicarbonate.

Cell-based in vitro experiments were conducted using the adult retinal pigment epithelial cell line ARPE-19. The cells were cultivated at 37 °C with 5% CO_2 atmosphere and 10% inactivated FCS (GIBCO, ThermoFisher Scientific, Germany) in DMEM/F12 medium supplemented with 10 000 U/ml of 1% penicillin-streptomycin. The cells were subcultured in 1:2 ratios once a week.

2.10.1. In Vitro Cell Viability Evaluation. Using an MTS assay in RGC-5 cells, we evaluated the cell viability of several systems (free EPOβ, blank HA-SH@liposomes, and EPOβ/HA-SH@liposomes). The results were compared to a blank control in which cells were cultivated in the culture media without any system. A 0.2 mm syringe filter was used to sterilize each system. For three days, cells (5×10^5 cells/100 μL solution) were grown on blank liposomes and EPOβ/HA-SH@liposomes in a well. The MTS reagent was used to evaluate the cytotoxicity following the manufacturer's instructions.[44] Sample absorbance was measured at 490 nm, and the following formula was used to determine the viability (%):

$$\text{Viability}(\%) = ([A]_{test}/[A]_{control}) \times 100 \tag{5}$$

In this case, $[A]_{control}$ represents the absorbance of the untreated cells, while $[A]_{test}$ represents the absorbance of the sample cells. Three experiments' worth of data are shown as mean ± standard deviation (SD).

2.10.2. Live-Dead Assay. Acridine orange (AO; Sigma, A8097) and propidium iodide (PI; Sigma, 81845) stock solutions were arranged as concentrates (670 μM AO, 750 μM PI) in PBS and stored at 4 °C in the dark until needed. A 24-well tissue culture plate was seeded with RGC-5 cells (2×10^5 cells/well), which were then cultivated for an entire night. After that, the cells were exposed to EPOβ/HA-SH@liposomes and blank liposomes for the entire day. To evaluate the live/dead cell ratio, the cells were rinsed and stained using a solution of approximately 0.67 μM AO and approximately 75 μM PI in PBS. A fluorescent microscope (IX71, Olympus, Japan) was used to record the live/dead fluorescence images following a 10 min dark incubation period at 37 °C.

https://doi.org/10.1021/acs.molpharmaceut.5c00079
Mol. Pharmaceutics 2025, 22, 2287−2305

2.11. EPOβ/HA-SH@liposomes Uptake Assay. In a 24-well tissue culture dish, RGC-5 cells (2×10^5 cells per well) were plated and allowed to incubate for the entire night. After that, the cells received a 24 h treatment with EPOβ/HA-SH@liposomes. Following treatment, the cells were fixed using 4% paraformaldehyde (PFA), washed, and permeabilized with 0.2% Triton-X100 for 30 min. Blocking was performed with 5% normal goat serum for one hour, after which the cells were exposed to an anti-Erythropoietin antibody for three hours at 37 °C. Following a PBS wash, the cells were treated for one hour with an antigoat Alexa Fluor secondary antibody and then counterstained with DAPI. We used a fluorescence microscope (IX71, Olympus, Japan) to image the immunostained cells.

2.12. HA-specific CD44 Receptor Interaction. To evaluate the effect of the CD44 receptor when HA and HA-SH are incorporated into liposomes, the uptake of these vectors was assessed using absorbance measurements, following a modified protocol based on a previous study.[38] Briefly, 50 000 ARPE-19 cells were seeded into 48-well plates with complete media. To investigate the interaction between the HA-CD44 receptor on ARPE-19 cells and HA and HA-SH on the surface of the liposomes, the uptake was studied after the initial saturation of the receptor. For this purpose, HA and HA-SH (10 kDa, 3 mg/mL) were dissolved in complete media and added to the cells for 2 h. Subsequently, the media were replaced, and 200 μL of FITC-labeled free liposomes, HA@liposomes, and HA-SH@liposomes were introduced. After a 24 h incubation period, the cells were thoroughly washed with PBS to remove nonabsorbed particles. This ensured that only the absorbance of particles internalized or adhered to the cell surface was measured. The absorbance of each sample was then recorded at 495 nm.

2.13. Animals. A total of 72 C57/BL6 mice, weighing an average of 20 ± 5 g, were employed. These mice were housed and cared for following the guidelines outlined in the ARVO for the use of animals in ophthalmic and visual research, adhering to the protocols established by Shahid Beheshti University's Animal Use and Care Committee (ethical approval code: IR.SBU.REC.1403.164). The mice were randomly divided into the defined groups and had access to food pellets and water *ad libitum*. The environmental conditions were maintained at 20 ± 2 °C with a relative humidity of 50−60%. Light and dark cycles were each set to 12 h.

2.14. Assessment of Liposomal Transfer Across Retinal Layers Following Intravitreal Administration. The retinal transfer of FITC-labeled HA-SH@liposomes was assessed following intravitreal injections in normal mice. This evaluation aimed to determine the transfer of liposomes resulting from the administration of these formulations into the eye. A volume of 3 μL of FITC-labeled HA-SH@liposomes was injected intravitreally. After 24 h, the eyes were examined for any signs of toxicity, including inflammation and redness, before being enucleated and evaluated through cross-sectioning.

2.15. Optic Nerve Crush (ONC). Anesthesia was administered to the animals using a 1:4 mixture of xylazine and ketamine. Intraorbital ONC was conducted as previously described.[45] Briefly, the optic nerve was carefully exposed just beneath the superior edge of the orbit and subjected to a 5 s compression using precision fine forceps (no. 5B forceps from World Precision Instruments) positioned 1 mm from the eyeball, taking care to avoid any damage to the retinal artery during the procedure.

2.16. Topical Administration of Nanoparticles, and Immunohistochemistry Assays. Two days after the optic nerve crush, each eye received one drop (100 μL) of the nanoformulation (1000 IU of EPOβ in 5 mL liposomes), which was applied topically five times within an hour. One group of animals was treated with HA-SH@liposomes containing EPOβ, while the other group received free EPOβ. For the control groups (untreated), PBS was used as the eye drops. Following the timeline, the animals were euthanized with an overdose of CO_2, and the enucleated eyes were immediately immersed in 4% PFA for an additional two hours (Sigma-Aldrich, P6148) before being stored in 30% sucrose for future cryosectioning. The mouse globes were then cryosectioned into 8 μm sections and mounted on Superfrost Plus slides (Thermo Scientific, 4951, Germany).

For immunostaining, the tissue sections were permeabilized using 0.5% Triton X-100 in PBS for 30 min, followed by blocking with 10% normal goat serum for one hour. The sections were then incubated overnight at 4 °C with a primary antibody in a blocking solution. After this, they were treated with a secondary antibody for one h at room temperature. Finally, the sections were stained with DAPI for 5 min and observed under a microscope (Olympus IX71, Olympus, Japan). A list of the antibodies used is provided in Table S2.

2.17. EPOβ Quantification. Since our study demonstrated the passage of EPOβ across the corneal and retinal barriers, the next step to further validate the efficacy of this administration method involved using a human erythropoietin ELISA kit (Abcam ab119522, Cambridge, England). The study involved four experimental groups to evaluate the passage of EPOβ across the ocular barriers. The groups included a control group (4 eyes) that received only PBS solution, a blank group (8 eyes) treated with HA-SH@liposomes without EPOβ, an EPOβ group (8 eyes) treated with the simple form of EPOβ, and an EPOβ/HA-SH@liposomes group (8 eyes) treated with EPOβ encapsulated in HA-SH@liposomes. EPOβ was applied topically in both its liposomal and simple forms using the same method as before (1000 IU of EPOβ in 5 mL liposomes). After 24 h, the mice were anesthetized, and the eyes were enucleated. The anterior sections were removed, and then the ocular tissues were lysed using RIPA buffer solution (Cat No.: DB9719, dnaBIOTECH, Iran) following the kit's instructions. The EPO levels in each eye were then measured using a microplate reader (FLUOstar Omega, BMGLabtech, Germany) at a wavelength of 450 nm, and comparative analysis was conducted.

2.18. Optokinetic Response Visual Acuity. Using an OptoDrum system (Striatech Technologies, Germany), the animals' spatial visual acuity was assessed 60 days after the injuries. The OptoDrum consists of black and white stripes rotating on four computer monitors arranged in a square configuration, with a camera mounted on an elevated platform at the center. The stripes rotate either clockwise or counterclockwise; clockwise rotation stimulates the left eye's optomotor reflex, while counterclockwise rotation stimulates the right eye's reflex. Initially, the stripes were rotated at a low spatial frequency, and the animals' reflexive head movements were observed to assess their ability to detect the moving stripes. The spatial frequency of the stripes was then gradually increased until the animals could no longer elicit the optomotor reflex. This method allowed the determination of

https://doi.org/10.1021/acs.molpharmaceut.5c00079
Mol. Pharmaceutics 2025, 22, 2287−2305

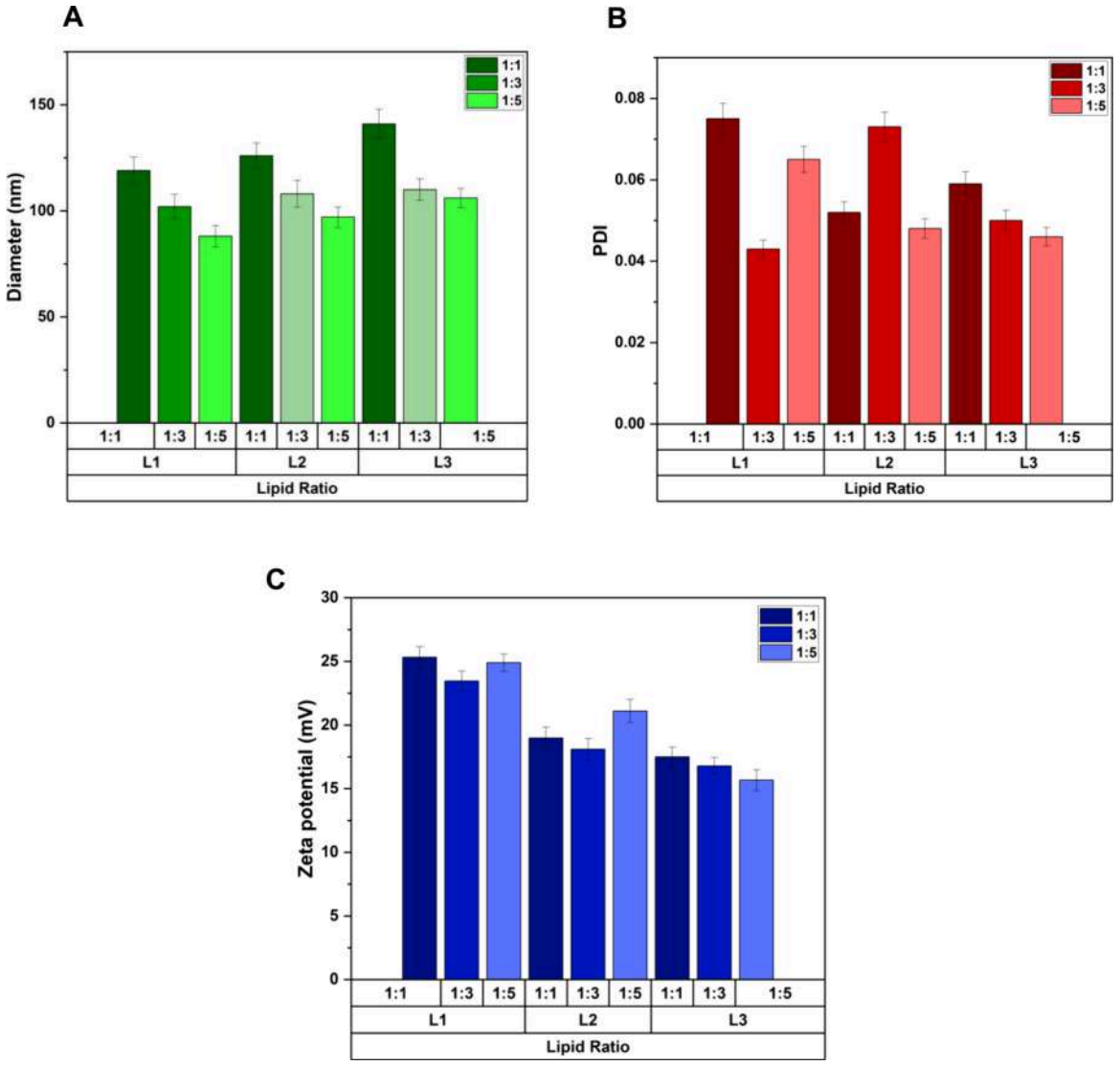

Figure 1. (A) The average diameter of the empty cationic liposomes at different FRRs. (B) The average PDI of the empty cationic liposomes at different FRRs. (C) The zeta potential of the empty cationic liposomes at different FRRs. L1, 50:25:25; L2, 55:25:20; L3, 55:30:15.

visual acuity, which was reported in cycles per degree (cycle/degree). The study involved four experimental groups to evaluate the animals' spatial visual acuity: a control group (8 eyes) that received only PBS, a blank group (8 eyes) treated with HA-SH@liposomes without EPOβ, an EPOβ group (8 eyes) treated with the simple form of EPOβ, and an EPOβ/HA-SH@liposomes group (8 eyes) treated with EPOβ encapsulated in HA-SH@liposomes.

2.19. Statistical Methods. Statistical analysis was conducted using Microsoft Office Excel (Microsoft, WA, USA) and GraphPad Prism version 6.0 (GraphPad Software, CA, USA). For in vivo assays, one-way ANOVA followed by Tukey's post-hoc test was used to determine statistically significant differences in group means, with a significance threshold of $p < 0.05$. Results were reported as means ± SD. In section 2.4, normality tests and two-way ANOVA were applied to evaluate the impact of FRR and lipid ratios. In section 2.8.2, normality tests and Repeated Measures ANOVA were used to analyze stability across time points.

3. RESULTS AND DISCUSSION

3.1. Preparation of EPOβ/HA-SH@liposomes Using Post-Microfluidics Conjugation Approach. *3.1.1. Synthesis of HA-SH.* The thiolated hyaluronic acid (HA-SH) was synthesized by using a carbodiimide-mediated chemical technique, where HA was modified with thiol groups to enhance mucoadhesive properties and facilitate conjugation with cationic liposomes. The synthesis involved activation of HA with EDCI/NHS, followed by a reaction with CSA·HCl. The final HA-SH product was purified by dialysis and lyophilization. The degree of thiolation (60.56%) was confirmed using the Ellman method,[46] UV spectroscopy (412 nm peak), and ^{1}H NMR (peaks at 2.65 and 2.75 ppm). Detailed synthesis and characterization data are provided in the Supporting Information (Scheme 1S).

3.1.2. Preparation and Optimization of Cationic Liposomal Formulation. Microfluidic technology was employed in this study to fabricate cationic liposomes with a diameter of less than 100 nm, a low PDI of under 0.05, high uniformity, and remarkable stability. The ideal formulation was achieved by varying the FRR and employing various lipid ratios, among

https://doi.org/10.1021/acs.molpharmaceut.5c00079
Mol. Pharmaceutics 2025, 22, 2287−2305

other formulation parameters that have been investigated. Controlling the various manufacturing process factors, including the FRR, which has a significant impact on the liposome's diameter and uniformity, is one of most potent functions of microfluidics. To examine the effects of varying the FRR on the liposome diameter, PDI, and zeta potential, various FRRs were examined for each lipid ratio. The results indicate that the diameter of the liposome and the FRR have an inverse relationship, as illustrated in Figure 1A. The diameter of the liposomes in all formulations (L1−L3) shows a notable reduction upon increasing the FRR from 1:1 to 1:3 to 1:5 (L1, 50:25:25; L2, 55:25:20; L3: 55:30:15). The presented outcome is consistent with the pattern of our earlier research,[47] and other studies in the field.[48] This reduction in particle size with an increasing FRR can be explained by understanding the mixing process parameters. Liposome formation primarily occurs due to lipid self-assembly upon mixing with an aqueous solution, a process referred to as nucleation. As the FRR increases, the final solvent concentration is reduced, minimizing particle infusion, also known as the Ostwald ripening phenomenon, and stabilizing liposomes at their initial size postnucleation. Therefore, the observed size reduction is attributed to diminished Ostwald ripening with higher FRRs.[49] Two-way ANOVA confirmed that both flow rate (P = 0.002) and lipid ratio (P = 0.021) significantly influenced liposome size, with smaller particles observed at higher flow rates and varying lipid compositions. The model, explaining 96.82% of the data variation, highlights the reliability of this method in customizing nanoparticle sizes through microfluidic optimization.

Incorporating the DOTAP lipid into the liposome's composition with the right ratio can provide a steric stabilization effect, especially for cationic liposomes. When combined with other lipids in the liposome formulation, DOTAP can help liposome stability by creating repulsive forces between positively charged lipids, thus preventing the aggregation or fusion of liposomes. DOTAP decreased the average diameter of multilamellar liposomes containing PC, irrespective of the length of the phospholipid chain and degree of unsaturation.[50] The similar pattern of a decrease in liposome size following the addition of DOTAP as a cationic lipid is supported by additional research in the literature.[51] On the other hand, although DOTAP can provide stabilization effects within a certain concentration range, increasing its mol % beyond appropriate levels can destabilize the lipid bilayer of the liposomes. High charge densities can lead to electrostatic repulsion between DOTAP molecules, which can disrupt the packing and stability of the lipid bilayer. The discrepant unstable population of L1 and the high PDI values seen in Figure 1B could have resulted from the DOTAP lipid mol % being inappropriate for the lipid ratio. Since there is no direct correlation between the DOTAP lipid content and liposome size, the primary objective was to determine the optimal concentration to achieve the necessary size and stability.

In FRR (1:5), for L1, the average diameter was 88 ± 1.23 nm with a PDI of 0.065. For L2 and L3, the average diameter was 97 ± 1.09 and 106 ± 1.05 nm, and the PDI average was 0.048 and 0.046, respectively. The PDI increases and the liposome diameter decreases when the DOTAP lipid mol % is increased from 15% for L3 to 25% for L1. This decrease in the liposome diameter is in line with previous research in the literature. The stability and reproducibility of the liposomal formulation were found to be significantly impacted by the ratio of the lipids to the DOTAP lipid. Lipid bilayers typically maintain stability through a delicate balance of hydrophobic interactions, van der Waals forces, and electrostatic interactions. This destabilization often occurs due to the higher positive charge density imparted by excessive amounts of DOTAP. The lipid bilayer's phase behavior may change when significant concentrations of DOTAP are added; this could lead to the onset of nonbilayer phases (such as micellar phases), which could collapse the bilayer structure.[52] The literature has reported that the lipid bilayer may become unstable if the DOTAP mol % is increased to inappropriate amounts. The findings (Figure 1B) indicate that coupling DOTAP lipids with SPC and DOPE in the L2 ratio produces a liposomal formulation with optimal diameter, excellent stability, and repeatability. In contrast, formulations with L1 and L3 ratios exhibited significant variability in particle size from day 0, low stability, and poor reproducibility. While microfluidic parameters like FRR play a crucial role in determining liposomal characteristics, the lipid ratio alone does not dictate diameter and homogeneity.

The optimal formulation for EPOβ encapsulation was L2 at a TFR of 10 mL/min and an FRR of 1:5, which achieved a small diameter, high homogeneity (PDI < 0.05), and good stability. However, two-way ANOVA revealed no significant effects of flow rate or lipid ratio on PDI (P-values of 0.752 and 0.747, respectively). Additionally, the model explained only 23.68% of PDI variation, indicating limited predictive ability based on these parameters.

Figure 1C presents the zeta potential values of free cationic liposomes with three lipid compositions (L1, 50:25:25; L2, 55:25:20; L3, 55:30:15) across flow rate ratios (FRR) of 1:1, 1:3, and 1:5. L1 consistently exhibited the highest zeta potential due to its higher DOTAP content, resulting in a stronger positive surface charge. However, no consistent trend in zeta potential was observed within individual formulations (L1, L2, or L3) across different FRRs, indicating complex interactions between lipid composition and flow rate conditions that affect the surface charge variability.

Two-Way ANOVA revealed that lipid composition significantly influences the zeta potential (P = 0.003, F = 33.12), with L1 contributing positively (P = 0.002). Conversely, FRR had no significant effect (P = 0.481, F = 0.88). The model explained 94.44% of the variability in the zeta potential, highlighting lipid composition as the dominant factor, while the FRR played a minimal role within the tested range.

3.1.3. Bench-Scale Production of EPOβ-Loaded Cationic Liposome Formulations and Encapsulation Efficiency. Small-diameter liposomes (<200 nm) were selected for their ability to minimize immune reactions and enhance drug delivery through increased surface area and cellular barrier penetration.[53,54] Using a toroidal mixer design and hydrodynamic focusing within a desktop NanoSynthesizer system, liposomes were fabricated with high efficiency. The system allowed precise control of parameters such as the flow rate ratio (FRR: 1:5 EtOH/D-PBS) and total flow rate (TFR: 10 mL/min), yielding liposomes with optimized lipid ratios (55:25:20 for DOTAP, SPC, and DOPE) and high encapsulation efficiency (>90%) of EPOβ. The liposomes were dialyzed postsynthesis to remove residual solvents. These formulations effectively addressed challenges associated with the weak membrane permeability of peptide drugs like EPOβ by encapsulating them within the liposomal structure.[55]

https://doi.org/10.1021/acs.molpharmaceut.5c00079
Mol. Pharmaceutics 2025, 22, 2287−2305

The L2 formulation (55:25:20 SPC/DOPE/DOTAP) demonstrates superior characteristics as a nanocarrier for EPOβ, including a small diameter (<0.05 μm), which enhances its functionality. Peptide drugs like EPOβ face challenges in membrane permeability due to factors such as peptide length and amino acid composition, limiting their therapeutic applications. Liposomes offer a solution by encapsulating EPOβ, addressing its weak membrane permeability.

The encapsulation of EPOβ in cationic liposomes via a microfluidic method is highly efficient and controllable. The strong electrostatic interaction between negatively charged EPOβ and positively charged liposomes contributes to an EE% exceeding 90% at a concentration of 1000 IU for L2 (Table 2).

Table 2. Characteristics of Liposomal Formulations for EPOβ Encapsulation.

formulation	composition	EPOβ concentration	DL%	EE%
L2	55:25:20 SPC/DOPE/DOTAP	1000 IU in 5 mL of liposome (1.68 μg/mL)	12%	>90%

The microfluidic technique ensures precise control, uniform liposome size, and scalability, outperforming traditional methods such as extrusion or thin-film hydration, which struggle to achieve high EE% for large or hydrophilic molecules like EPOβ (typically < 50%). This highlights the microfluidic method as a superior approach for producing protein-encapsulated liposomes.[56,57]

3.1.4. EPOβ/HA-SH@liposomes. The negatively charged vitreous cannot strongly electrostatically connect to the EPOβ due to its negative charge.[58] Normally, the vitreous serves as a significant barrier that prevents drugs from diffusing into the posterior section.[59] By shielding pharmaceuticals from the ocular environment and improving drug penetration via biological ocular barriers, mucoadhesive nanoparticles can increase the intraocular concentration and bioavailability of pharmaceuticals. Since they have a stronger bond with the ocular mucosa, they are crucial as carriers for topical ocular delivery.[28]

The purpose of this work is to develop HA-SH-based mucoadhesive liposomes for the administration of an EPOβ utilizing a postmicrofluidics conjugation technique. The main mechanism behind HA-SH's enhanced mucoadhesive qualities is the formation of disulfide bonds between the mucus's cysteine-rich residues and the polymer backbone's sulfhydryl moieties. Furthermore, the human conjunctiva, corneal epithelial cells, and retinal pigment epithelium are among the ocular cells where HA binds to the CD44 receptors.[60] Covalent modification through chemical processes is a common method of attaching HA molecules to the surface of nanoparticles.[61] Nevertheless, in certain situations, these interactions can result in toxicity. Without the need for chemical reagents, electrostatic attraction is a straightforward and manageable process. HA is a negatively charged linear polymer since every disaccharide unit contains a carboxyl group.[62] In this study, HA-coated nanoliposomes were prepared by the electrostatic interaction between the negatively charged HA and DOTAP, a cationic phospholipid. To accomplish this goal, we propose a well-proven mucoadhesive liposome system in which HA-SH attaches itself in a 55:25:20 molar ratio to the surface of cationic liposomes made of SPC, DOPE, and DOTAP. The production of these liposomes, which have an estimated diameter of 97 nm, is done by a microfluidic technique that guarantees their stability at pH 7.4.

There are three stages involved in the manufacture of EPOβ/HA-SH@liposomes. First, sulfhydryl ligands were attached to naturally existing HA to create HA-SH, as explained in section 2.3. Next, using a microfluidic hydrodynamic flow-focusing technique, liposomes with a weight ratio of 55:25:20 were made from SPC, DOPE, and DOTAP. Electrostatic attraction was then used to load negatively charged EPOβ into the cationic liposomes. Finally, for 60 min, the cationic liposomes and the anionic HA-SH were combined at a concentration of 0.05% (w/v) and gently swirled (Figure 2A). After production, DLS measurements revealed that the EPOβ/HA-SH@liposomes exhibited a surface zeta potential of -13.7 ± 0.7 mV and a diameter of 144.1 ± 1.3 nm (PDI = 0.09 ± 0.01). The approximately 30 nm increase in diameter of EPOβ/HA-SH@liposomes compared to bare liposomes is attributed to the adsorption of HA-SH onto the liposomal surfaces. Changes in zeta potential further validate this process. Initially, the SPC/DOPE/DOTAP liposomes exhibited a cationic charge of +17.7 mV, which shifted to −14.7 mV after HA-SH coating, confirming the attachment of negatively charged hyaluronic acid. Encapsulation of EPOβ further reduced the zeta potential to −20.66 mV.

TEM imaging revealed the structural details, showing a visible HA-SH layer on the liposome surface (Figure 2B, C). FE-SEM images (Figure 2D) confirmed the successful preparation and coating of HA-SH@liposomes.

The synthesized HA-SH was successfully attached to the surface of the cationic liposomes. As illustrated in Supporting Information, Figure 1S, a slight shift in the maximum UV−visible spectrum peak was observed, from λ = 495 nm for free liposomes to λ = 500 nm for HA@liposomes and λ = 505 nm for HA-S@liposomes. This spectral shift confirms the successful binding of HA-SH to the liposome surface. Across all batches prepared in this study, the binding efficiency of HA-SH to the liposome surface was approximately 76%.

3.1.5. Permeation Study of EPOβ. The in vitro drug permeation profiles of EPOβ/HA-SH@liposomes, EPOβ/liposomes, and the free drug were evaluated by using a MicroBCA Kit Assay (Figure 3). The study was conducted in a simulated physiological environment at pH 7.4 to mimic normal tissue conditions. In simulated tear fluid (37 °C, pH 7.4), EPOβ/HA-SH@liposomes exhibited an initial burst permeation of 20−30% within the first 15 min, followed by a sustained permeation of approximately 76.34% over 72 h. Their DL% and EE% were determined to be 17.4 ± 0.1% and 90.4 ± 0.3%, respectively.

In comparison, after 72 h, EPOβ/liposomes permeated 88.85% of the drug, while HA-SH@liposomes showed a slightly slower permeation of 76.34%, reflecting the stabilizing effect of the thiolated hyaluronic acid modification. The free drug, in contrast, permeated more than 80% within the first few hours, demonstrating its rapid and uncontrolled permeation.

These results highlight the advantages of HA-SH@liposomes, which provide more controlled and sustained permeation compared to the free drug, although the unmodified liposomes exhibited a slightly higher permeation percentage over time. The thiolated hyaluronic acid modification enhances drug retention and stabilizes the liposomal structure, making HA-SH@liposomes promising

https://doi.org/10.1021/acs.molpharmaceut.5c00079
Mol. Pharmaceutics 2025, 22, 2287−2305

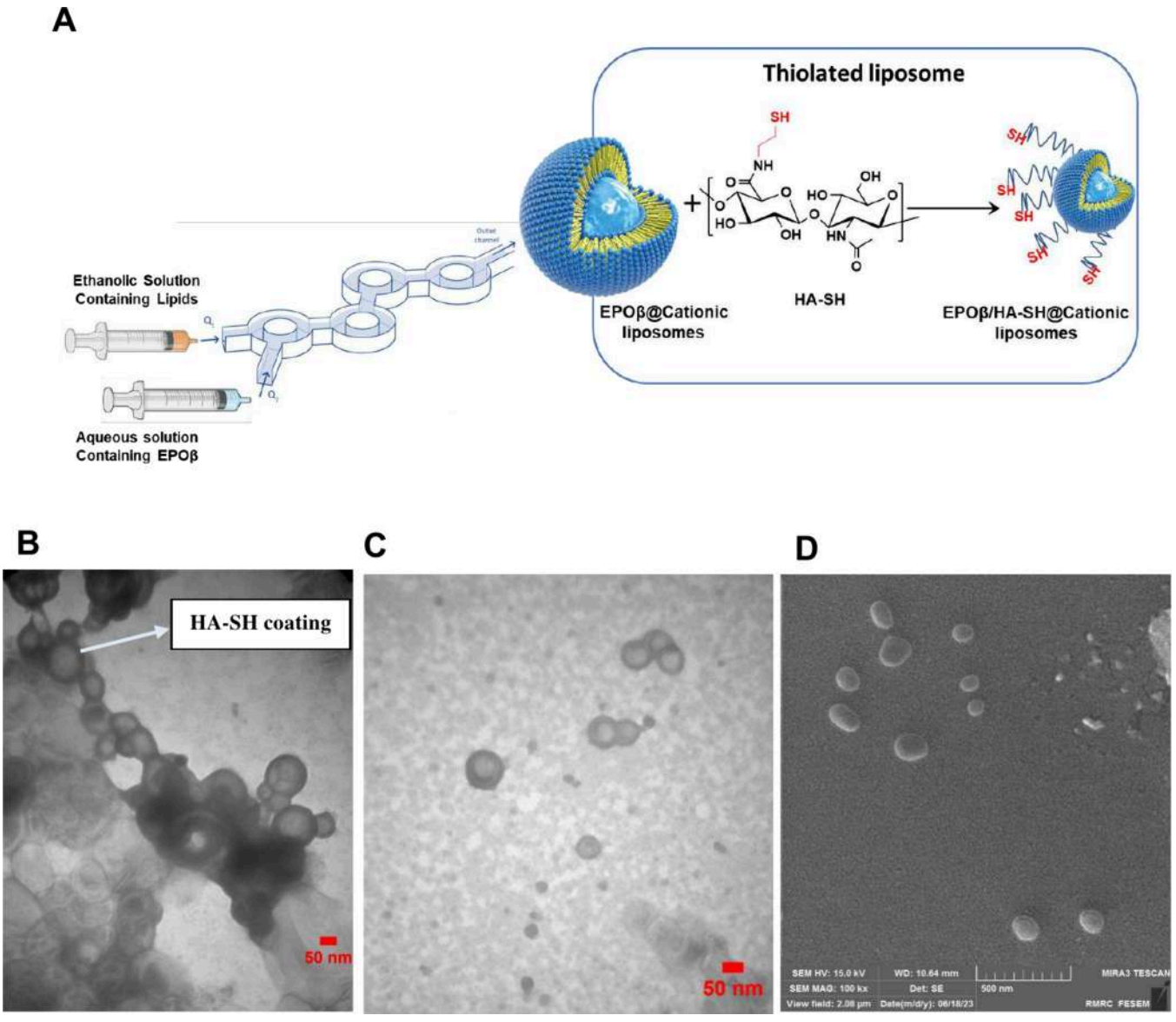

Figure 2. Validation and characterization of EPOβ/HA-SH@liposomes (formulation L2). (A) Schematic representation of microfluidics-based encapsulation of a hydrophilic drug (EPOβ) into a clinical cationic liposome formulation (toroidal micromixer adapted from Belliveau et al.[63]) and then the postmicrofluidic conjugation approach for the preparation of EPOβ/HA-SH@liposomes. (B, C) TEM micrographs of HA-SH@liposomes. (D) FE-SEM micrograph of HA-SH@liposomes.

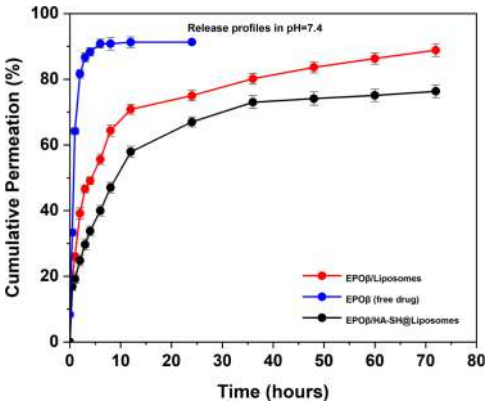

Figure 3. EPOβ permeation study from EPOβ/HA-SH@liposomes, EPOβ/liposomes, and the free drug in the simulated physiological environment of normal tissues (pH 7.4).

candidates for prolonged and controlled drug delivery applications.

The drug permeation kinetics of EPOβ from the free drug, EPOβ/liposomes, and EPOβ/HA-SH@liposomes were evaluated using four kinetic models: zero-order, first-order, Higuchi, and Korsmeyer–Peppas. Among these, the Korsmeyer–Peppas model consistently provided the best fit (R^2 = 0.99) across all formulations, highlighting its relevance in describing the permeation mechanisms (Supporting Information, Table 2S). For the free drug (EPOβ), the Korsmeyer–Peppas model showed the strongest correlation (R^2 = 0.99) with an n-value of 0.1, indicative of Fickian diffusion. This suggests that permeation is dominated by passive diffusion into the surrounding medium without any structural barriers or additional permeation mechanisms. The Higuchi model, with a moderate R^2 = 0.60, further supports diffusion as a contributing factor, but it is not the sole mechanism. Neither the zero-order nor the first-order models provided an adequate

https://doi.org/10.1021/acs.molpharmaceut.5c00079
Mol. Pharmaceutics 2025, 22, 2287−2305

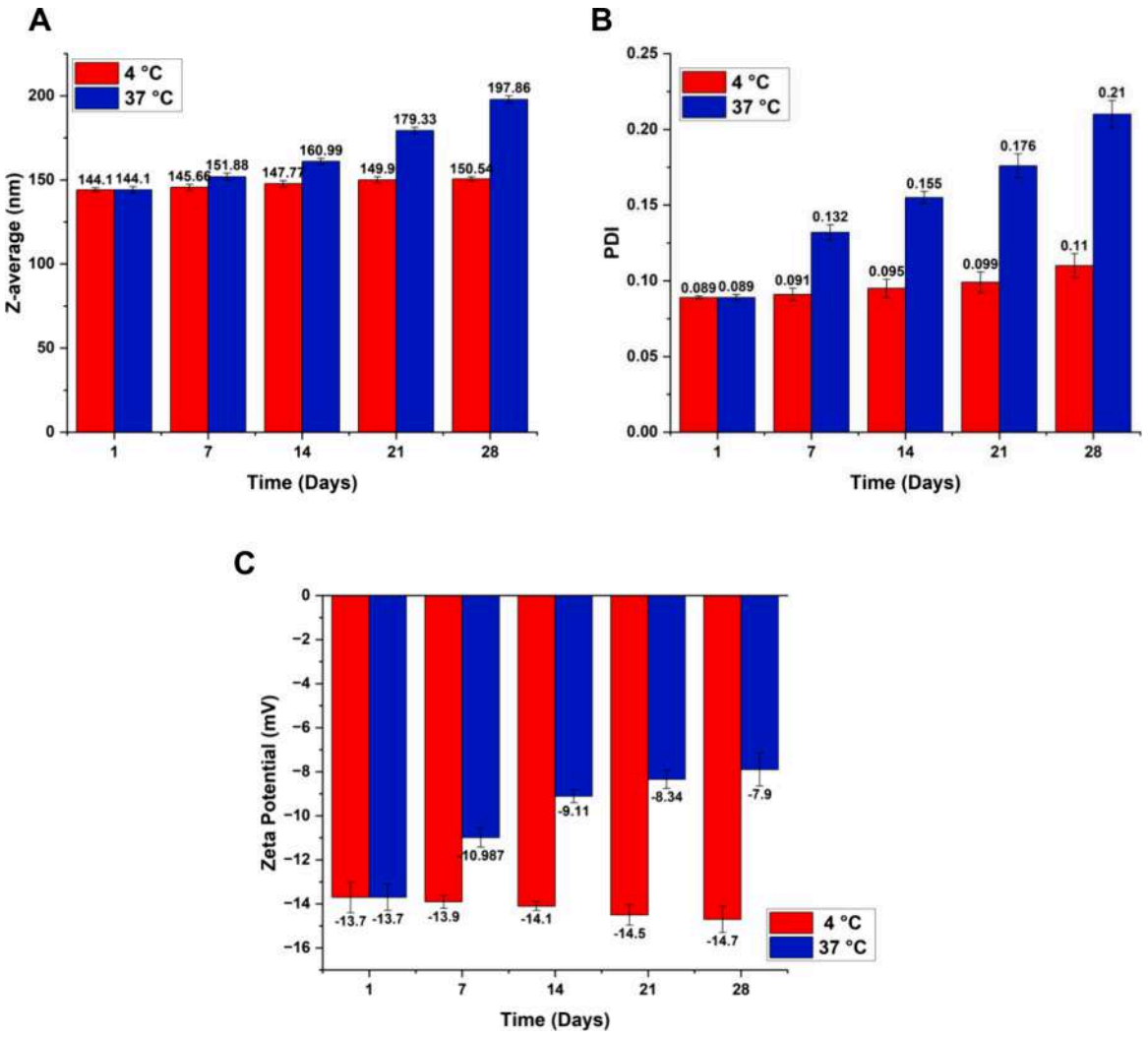

Figure 4. Physical stability of HA-SH@liposomes stored at 4 and 37 °C over 4 weeks. (A) Z-average: the hydrodynamic diameter of the liposomes, (B) PDI indicating size distribution uniformity, and (C) zeta potential representing surface charge stability. Samples were analyzed immediately after preparation and during storage without filtration. Data are presented as mean ± SD (n = 5 independent formulations, with each result being the mean of N = 5 measurements).

description of the permeation, ruling out constant-rate- or concentration-dependent processes. The poor performance of the zero-order and first-order models for EPOβ/liposomes, as illustrated in Supporting Information, Figure 2S(A, B), indicates that the permeation is not constant nor exclusively reliant on drug concentration. The Higuchi model also aligned well, emphasizing diffusion as the dominant mechanism (Supporting Information, Figure 2S(C)). However, the Korsmeyer−Peppas model offered the best fit (R^2 = 0.99) with an n-value of 0.23. This indicates a mixed mechanism where Fickian diffusion predominates but is complemented by additional processes, potentially due to the structural relaxation or slight reorganization of the liposomal membrane (Supporting Information, Figure 2S(D)). As illustrated in Supporting Information, Figure 2S(E, F), the weaker fit of the zero-order (R^2 = 0.78) and first-order (R^2 = 0.65) models confirms that the permeation mechanism is more complex than simple zero-order kinetics or a concentration-driven process. The Korsmeyer−Peppas model demonstrated the highest accuracy (R^2 = 0.99) with an n-value of 0.31, pointing to an anomalous diffusion mechanism. This suggests that a combination of Fickian diffusion and additional factors, such as potential swelling or minor erosion of the HA-SH-modified liposomal surface, governs the permeation. The Higuchi model (R^2 = 0.92) further supports diffusion-driven permeation as a key component (Supporting Information, Figure 1S(G, H)). Diffusion is the primary mechanism regulating permeation kinetics, with various levels of supplementary contributions based on the formulation. The modification with HA-SH in EPOβ/HA-SH@liposomes appears to introduce secondary mechanisms that support sustained and controlled permeation, as evidenced by the higher nnn-value compared to that of unmodified liposomes. The HA-SH-modified system provides enhanced control over drug permeation through a diffusion-dominated but multifaceted mechanism.

3.2.5. Stability. 3.2.5.1. Physical Stability. The integrity and effectiveness of liposomal formulations are dependent on the stability of the liposomes. Surface charge (zeta potential) and size change (aggregation) are used to assess the physical stability of liposomes. The zeta potential is a measure of a particle's colloidal stability. Greater stability is indicated by a greater absolute value of the zeta potential, which is higher when particle charge is high enough to produce repulsion between nanoparticles and keep them from accumulating.[64]

https://doi.org/10.1021/acs.molpharmaceut.5c00079
Mol. Pharmaceutics 2025, 22, 2287−2305

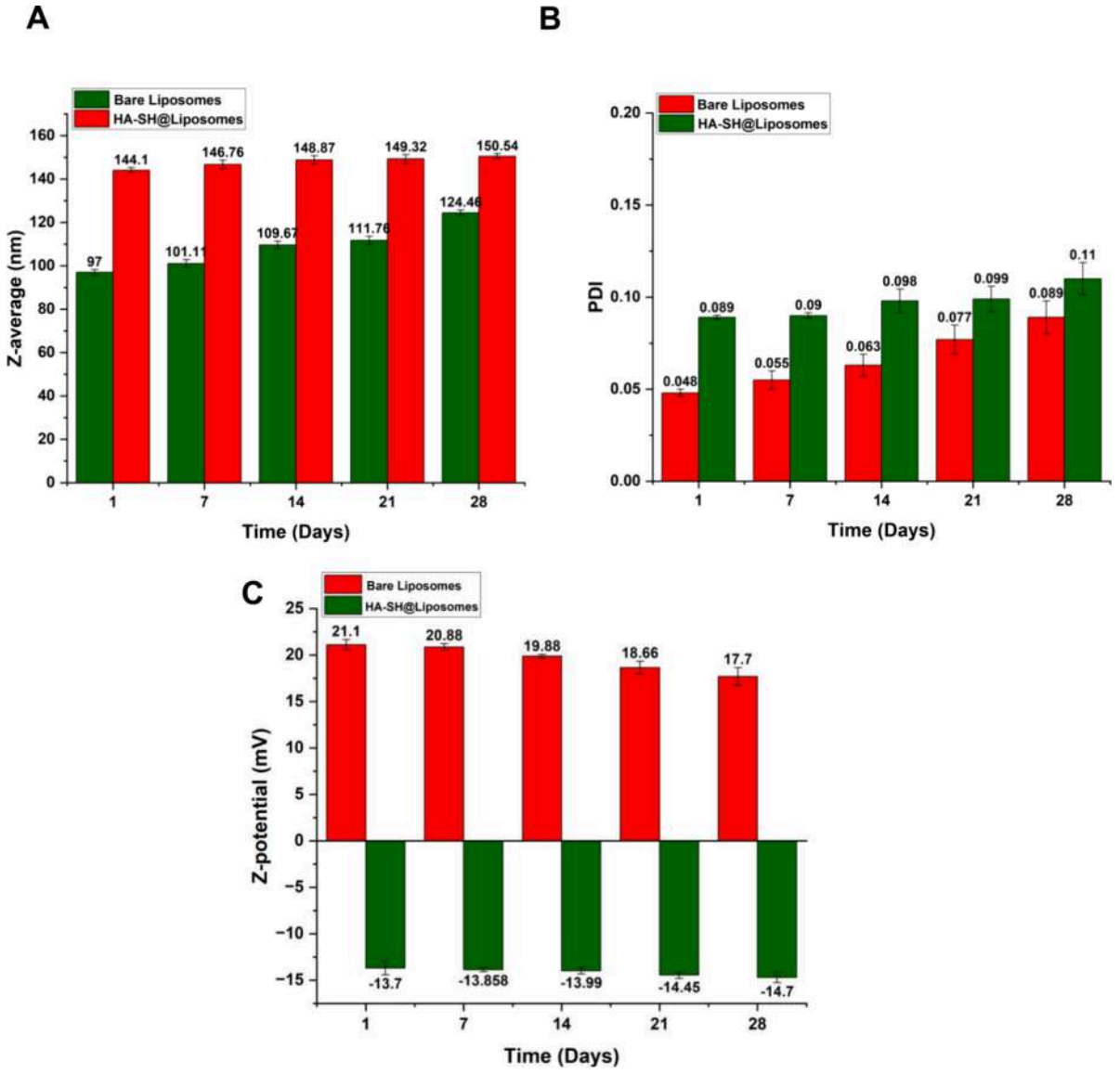

Figure 5. Chemical stability assessment of bare liposomes and HA-SH@liposomes stored for 28 days at 4 °C. (A) Z-average (particle size), (B) PDI, and (C) zeta potential measured at different time points (1, 7, 14, 21, and 28 days). Results are expressed as mean ± SD from 5 independent formulations (n = 5), with each formulation measurement repeated five times (N = 5). Notably, no filtration was performed on the samples after production or prior to measurements.

The Z-average size, PDI, and zeta potential were measured several times over a four-week period in order to examine the physical stability of the HA-SH@liposomes formulations developed in this investigation, which were stored at 4 and 37 °C immediately after production (Figure 4). The HA-SH@liposomes stored at 4 °C exhibited a minimal increase in particle size, as determined by DLS analysis, increasing from 144.1 ± 1.3 to 150.54 ± 0.33 nm over the storage period (Figure 4A). In contrast, the HA-SH@liposomes stored at 37 °C experienced a significant increase in particle size, from 144.1 ± 1.3 to 197.9 ± 0.76 nm, indicating potential aggregation or fusion of particles. Repeated Measure ANOVA revealed that temperature significantly influenced liposome size (P = 0.088) more than time (P = 0.326). The PDI data (Figure 4B) demonstrated a trend consistent with the particle size findings, where the samples stored at 4 °C displayed the smallest change in PDI, ranging from 0.09 ± 0.005 to 0.11 ± 0.003, suggesting a more uniform particle size distribution. However, at 37 °C, the PDI increased significantly from 0.09 ± 0.01 to 0.21 ± 0.01, indicating a loss of size homogeneity. Repeated Measures ANOVA for PDI data showed that temperature had a statistically significant effect on the particle size distribution (P = 0.031). The coefficient for 37 °C (0.0278) indicates higher PDI values at elevated temperatures compared to 4 °C. The zeta potential results (Figure 4C) revealed minimal changes in surface charge at 4 °C, with values slightly shifting from −13.7 ± 0.7 mV to −14.7 ± 0.6 mV, reflecting good stability. At 37 °C, the zeta potential decreased substantially from −13.7 ± 0.7 mV to −7.9 ± 0.9 mV over time, suggesting a loss of electrostatic repulsion and reduced colloidal stability under elevated temperature conditions. These findings collectively highlight that storage at 4 °C ensures better physical stability of HA-SH@liposomes compared to that at 37 °C. ANOVA results indicate that temperature significantly affects the zeta potential of liposomes (P = 0.028), with higher zeta values observed at 37 °C

https://doi.org/10.1021/acs.molpharmaceut.5c00079
Mol. Pharmaceutics 2025, 22, 2287−2305

compared to 4 °C. Time (day) showed no significant effect (P = 0.725). The model explains 77.17% of the variability in zeta, though the adjusted R^2 value (48.63%) suggests a modest fit, indicating that other factors may also influence the zeta potential.

Drug leakage is a crucial marker of the physical stability of liposomes, as it directly impacts the retention and controlled permeation of the encapsulated drug. In this study, liposomes stored at 4 °C exhibited significantly lower drug leakage (5.88 ± 0.48%) compared to those stored at 37 °C (26.68 ± 0.33%). These results suggest that lower storage temperatures minimize the encapsulated drug's escape by maintaining the integrity of the liposomal structure. At elevated temperatures, such as 37 °C, the lipid bilayer becomes more fluid and permeable, which can compromise the structural stability of the liposomes. This leads to increased drug leakage and a corresponding reduction in the overall stability over time.

3.2.5.2. Chemical Stability. The oxidation of lipids in vesicular systems can be avoided by coating liposomes with a polymer, enhancing their chemical stability. After being coated with HA-SH, the generated liposomes were compared to liposomes made with the same composition but without coating to determine whether one had greater chemical stability against oxidation.[65] The HA-SH coating was thought to have a high zeta potential value, which caused liposomes to repel one another electrostatically. Due to electrostatic repelling forces, which also reject the transition metals in charge of oxidizing lipids, this prevents vesicles from coalescing. The outcomes demonstrated the effectiveness of the HA-SH coating on liposomes in preventing lipid oxidation. Still, uncoated liposomes also demonstrated durability against oxidation, which is explained by soy PC's antioxidant properties. Therefore, the coating and antioxidant combination improved the durability of the liposomes and can be investigated as a great way to address the liposome oxidation problem throughout the storage period. The study's bare liposomes and HA-SH@liposomes formulations were stored at 4 °C immediately after production to assess their chemical stability. Over four weeks, measurements of zeta potential, PDI, and Z-average size were performed (Figure 5). The DLS analysis showed that the particle size of HA-SH@liposomes increased slightly from 144.1 ± 1.3 to 150.54 ± 0.33 nm. In contrast, bare liposomes exhibited a more significant size increase from 97 ± 1.09 to 124.4 ± 0.85 nm under the same storage conditions (Figure 5A). Repeated Measures ANOVA shows that polymer-coated liposomes (HA-SH@liposomes) are significantly larger than bare liposomes, with a highly significant p-value (p < 0.001) and a large F-value (109.77), indicating the strong impact of the polymer coating on liposome size. Notably, HA-SH@liposomes demonstrated the smallest change in PDI, suggesting greater uniformity in the particle size distribution over time (Figure 5B). Repeated Measures ANOVA reveals significant effects of both time (day) and group on the PDI. The day factor (P = 0.035) indicates meaningful changes in PDI over the storage period, emphasizing the influence of storage duration on liposome stability. Zeta potential analysis revealed minimal changes at 4 °C, with HA-SH@liposomes showing a slight decrease from −13.7 ± 0.7 to −14.7 ± 0.6 mV, while bare liposomes exhibited a reduction from +21.1 ± 2.3 to +17.7 ± 0.8 mV (Figure 5C). These results suggest that incorporating HA-SH improves the chemical stability of liposomes over extended storage periods compared to bare liposomes. Repeated Measures ANOVA indicates a significant difference in zeta potential between groups (bare liposomes vs HA-SH@liposomes, p < 0.001), with the model explaining 99.92% of the variability. However, the effect of time (day) was not significant (P = 0.140), indicating minimal changes over time.

3.3. Mucoadhesive Studies. *3.3.1. Viscosity Measurements.* A study using an Ostwald viscometer was conducted to evaluate the viscosity of the products and investigate the interaction between free liposomes, HA@liposomes, and HA-SH@liposomes eye drop solutions in the presence of mucin. The results, presented in Table 3, indicate that HA-SH@liposomes exhibit significantly higher viscosity compared to that of HA@liposomes. Furthermore, an increase in viscosity was observed in the presence of mucin for all formulations compared to their individual viscosities. This increase was particularly pronounced for HA-SH@liposomes, which exhibited a viscosity of 107 mPa·s compared to 59 mPa·s for HA@liposomes.

Table 3. Viscosity Values and Mucoadhesive Index for HA@liposomes and HA-SH@liposomes in the Absence and Presence of Mucin 5% (w/w)[a]

formulations	viscosity (mPa·s)	mucoadhesive index (%)
free liposomes	5.8 ± 0.4	
HA@liposomes	6.8 ± 0.1	
HA-SH@liposomes	10.8 ± 0.2	
mucin 5%	26.0 ± 0.9	
liposomes + mucin 5%	33.20 ± 0.1	4.4%
HA@liposomes + mucin 5%	59.0 ± 0.4	79.88%
HA-SH@liposomes + mucin 5%	107.0 ± 0.9	190.98%

[a]Mean ± SD, n = 3.

The mucoadhesive index was calculated for the HA@liposomes + mucin and HA-SH@liposomes + mucin solutions to evaluate the enhanced mucoadhesive strength resulting from interactions between the polymer and mucin (Table 3). Notably, the liposomes + mucin solution also demonstrated higher viscosity than the individual liposomes due to their cationic nature, which promotes stronger interactions with mucin.

3.3.2. Zeta Potential. The zeta potential analysis highlights the mucoadhesive properties of the studied systems (Figure 6). Liposomes exhibited a positive zeta potential (+21.1 mV), whereas HA-SH@liposomes showed a strongly negative zeta potential (−19.8 mV), attributed to the anionic nature of hyaluronic acid due to its carboxylic groups. Mucin also demonstrated a negative zeta potential (−11.3 mV), consistent with its oligosaccharide chains bearing carboxyl and sulfate groups. When mucin was added to both liposomes and HA-SH@liposomes, the zeta potential became more negative, indicating strong electrostatic interactions. This effect was more pronounced in the HA-SH@liposomes + mucin system, reflecting enhanced mucoadhesive properties due to complementary charges. A stability study over 1 h confirmed that these interactions remained consistent, suggesting the potential of these systems for sustained drug delivery through mucosal surfaces. The observed zeta potential values align with the existing literature, reinforcing the findings.

3.4. In Vitro Biocompatibility and Cellular Uptake. The in vitro biocompatibility of free EPOβ, blank HA-SH@liposomes, and EPOβ/HA-SH@liposomes on the normal

https://doi.org/10.1021/acs.molpharmaceut.5c00079
Mol. Pharmaceutics 2025, 22, 2287−2305

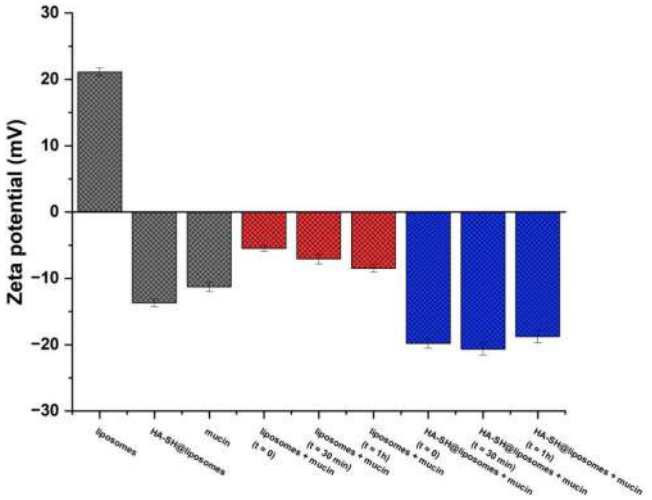

Figure 6. Determination of zeta potential for liposomes, HA-SH@liposomes, mucin 5%, and with mucin, absolute values (mean ± SD, n = 3).

RGC-5 cell line was assessed by using the MTS assay. The results showed no significant cytotoxicity compared to the control group (Figure 7A).

In addition to the MTS assay, the results from the delivery of EPOβ/HA-SH@liposomes were further confirmed using a fluorescence-based live/dead staining assay (Figure 7B). The live/dead assay allows for the simultaneous visualization of live and dead cells. The fluorescence-based live/dead staining assay

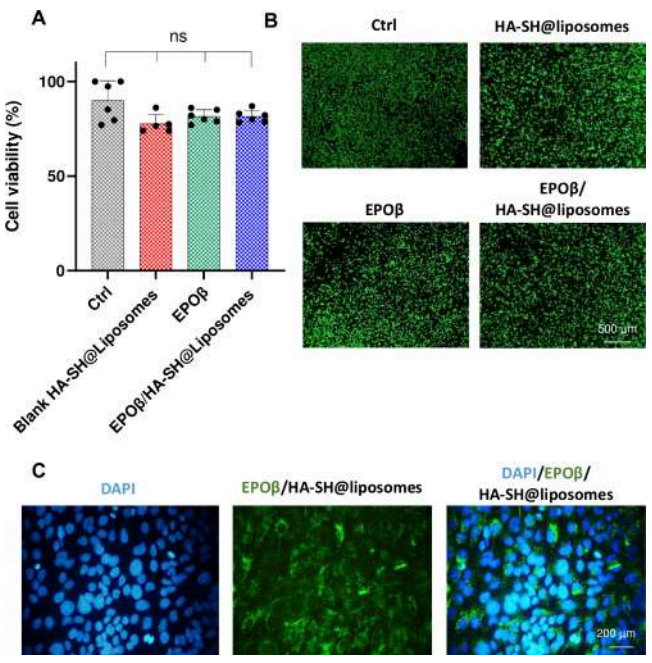

Figure 7. (A) Cytotoxicity evaluation by MTS assay on a RGC-5 cell line using different samples as shown (mean ± SD, n = 6) and after incubation with blank HA-SH@liposomes and EPOβ/HA-SH@liposomes. (B) Live and dead assessment using the RGC5 cell line. As depicted in this panel, the absence of red spots indicates no cell death, and the presence of green spots in all fluorescence images signifies the viability of cells, demonstrating the biocompatibility of EPOβ, EPOβ/HA-SH@liposomes, and HA-SH@liposomes. (C) The uptake of recombinant erythropoietin in the cytoplasm of RGC5 cells has been confirmed.

provides additional confirmation that both EPOβ/HA-SH@liposomes and HA-SH@liposomes are biocompatible, as evidenced by the absence of cell death and the presence of viable cells in treated samples the same as control. This highlights the promise of these liposomal systems for safe and effective drug delivery applications Furthermore, the study evaluated RGC-5 cells' uptake of recombinant EPO, with an emphasis on the EPOβ/HA-SH@liposomes formulation. After 24 h of exposure, most cells showed internalization of EPOβ, as visualized through immunostaining techniques. EPOβ was specifically stained within the cells, while nuclei were counterstained with DAPI, as illustrated in Figure 7C. These results highlight the potential of EPOβ/HA-SH@liposomes as a biocompatible and efficient therapeutic delivery technology.

3.5. Cell Interaction of Liposomes, HA@liposomes, and HA-SH@liposomes. Statistically significant differences were observed in the uptake profiles of different liposome formulations, likely due to the saturable nature of HA and HA-SH uptake via the CD44 receptor. To investigate this effect, CD44 receptors on ARPE-19 cells were saturated before a 2 h incubation with fresh media containing 200 μL of free liposomes, HA@liposomes, or HA-SH@liposomes. The results, as shown in Supporting Information, Figure 3S(A) and Figure 8, demonstrate that receptor saturation significantly reduced the uptake of HA@liposomes and HA-SH@liposomes, which rely on receptor-mediated mechanisms for cellular entry.

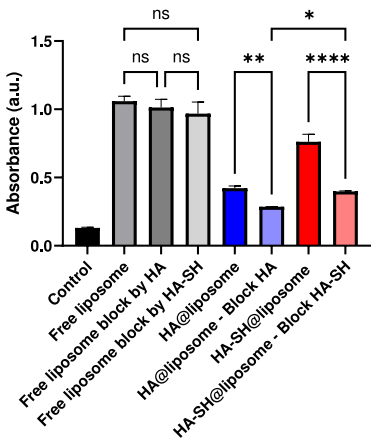

Figure 8. Absorbance comparison of different liposome formulations under various conditions. The bar graph shows the absorbance (a.u.) of free liposomes, liposomes blocked by HA or HA-SH, and HA@liposome/HA-SH@liposome formulations with and without HA or HA-SH blocking. Statistical significance is marked as ns (not significant), *p < 0.05, **p < 0.01, and ****p < 0.0001. Error bars represent the mean ± SD (n = 4).

In contrast, free cationic liposomes exhibited no significant reduction in uptake and reached higher intracellular levels, indicating their reliance on nonspecific pathways for uptake. This enhanced uptake is attributed to the cationic nature of free liposomes, which facilitates electrostatic interactions with the negatively charged cell membrane. These interactions promote adhesion and subsequent diffusion through the cell wall. Additionally, the lipid composition of the free liposomes, including SPC, DOPE, and DOTAP, enhances these interactions. DOTAP provides a positive charge, while DOPE contributes fusogenic properties that further aid membrane interactions.[66]

https://doi.org/10.1021/acs.molpharmaceut.5c00079
Mol. Pharmaceutics 2025, 22, 2287−2305

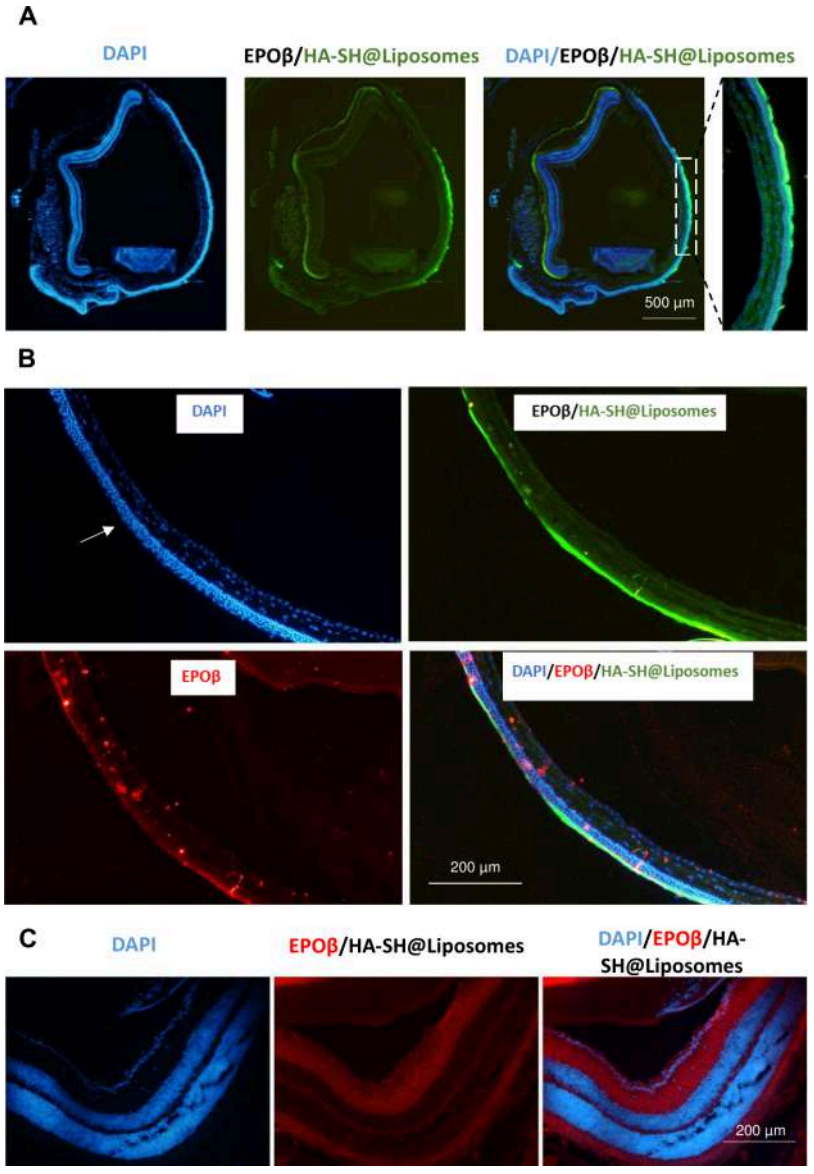

Figure 9. (A, B) Co-localization of FITC-labeled HA-SH@liposomes (incubated with the Alexa Fluor 546-tagged secondary antibody fragment) in mice ocular structures 3 and 24 h after five topical applications. (C) Co-localization EPOβ/HA-SH@liposomes incubated with the Alexa Fluor 546-tagged secondary antibody fragment in mice ocular posterior segments.

Among the coated liposomes, HA-SH@liposomes demonstrated significantly higher cellular uptake compared with HA@liposomes, indicating that HA-SH-functionalized liposomes exhibit a stronger affinity for CD44 receptors due to the enhanced receptor-binding properties of HA-SH. However, the overall uptake of both HA@liposomes and HA-SH@liposomes was substantially lower than that of free cationic liposomes. This difference highlights the distinction between nonspecific electrostatic interactions, which drive the greater uptake of free liposomes, and the receptor-mediated pathways favored by HA and HA-SH coatings, which depend on CD44 receptor availability. In the Supporting Information, Figure 3S(B) further confirms these findings with fluorescence microscopy images showing the cellular uptake of HA@liposomes and HA-SH@liposomes, both with and without HA or HA-SH blocking. In these merged images, DAPI staining (blue) marks the nuclei, while green fluorescence indicates the presence of liposomes. Panels showing strong green fluorescence in HA@liposomes (a) and HA-SH@liposomes (b) demonstrates uptake, whereas blocking with HA (c) or HA-SH (d) significantly reduces fluorescence, confirming the inhibitory effects of receptor blocking on liposome internalization.

3.6. Topical Administration of FITC-Labeled Liposomes. EPOβ was previously thought to be only a hematopoietic cytokine produced by the adult kidney and fetal liver, but over the past few years numerous studies have provided evidence of additional roles for EPOβ in various tissues.[67] It was found that the brain[6] and the retina[7] are new EPO-secreting organs that also exhibit EPO receptors.[9] The antiapoptotic, angiogenic, anti-inflammatory, antioxidant, and neuroprotective properties of EPO in the retina and other ocular tissues are described in a recent review article.[68] EPOβ was chosen for this investigation with the goal of serving as a neuroprotective agent to aid in the treatment of neurodegenerative diseases, since it is a recombinant human EPO that is frequently utilized in medical practice.

https://doi.org/10.1021/acs.molpharmaceut.5c00079
Mol. Pharmaceutics 2025, 22, 2287−2305

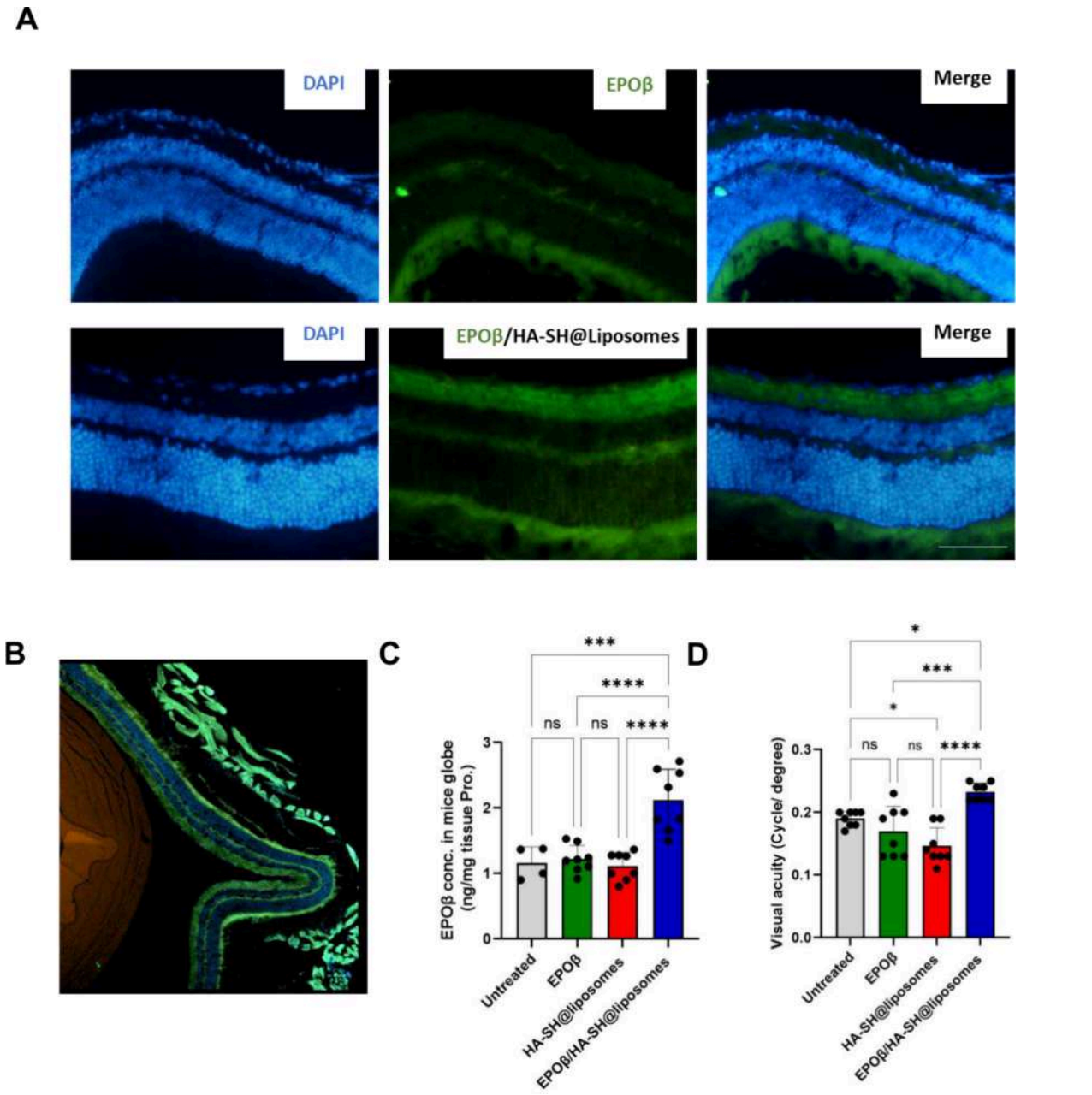

Figure 10. (A) Co-localization of free EPOβ and EPOβ/HA-SH@liposomes in mice ocular posterior segments 24 h after five topical applications within an hour (incubated with the Alexa Fluor 488-tagged secondary antibody fragment). (B) Confocal microscopy photomicrographs showing cross sections of the treated eye. (C) The levels of EPOβ in the entire eyeball measured by ELISA. (D) Graph showing that EPOβ/HA-SH@ liposomes topical administration in the injured retina significantly preserves visual acuity 2 months after administration, as assessed using the optomotor test. P = 0.001, data represent mean ± SD, n = 8 per group.

To assess the in vivo retinal barrier penetration capability of FITC-labeled HA-SH@liposomes, we performed intravitreal administration in normal mice. Our results indicate that these liposomal formulations are well-tolerated, with no significant inflammation observed, apart from a brief period of mild vitreous opacity. This underscores the potential of these liposomes for safe ocular drug delivery applications (Supporting Information, Figure 4S) while also demonstrating that the FITC-labeled HA-SH@liposomes can penetrate the neural retinal layers.

Based on these findings, we proceeded to assess the distribution of EPOβ and liposomes across the mouse's entire eyeball at various intervals following administration of FITC-labeled HA-SH@liposomes as eyedrops (Figure 9). According to the longitudinal section of mouse eyes, 3 h after the eyedrop was applied, mice treated with FITC-labeled HA-SH@ liposomes showed notable fluorescent signals from corneal epithelium to corneal endodermis (Figure 9A, B), whereas relatively weak fluorescence signals were found in the cornea of mice treated with free EPOβ (data not shown).

Having confirmed that the nanoparticles can pass through the corneal epithelium, we proceeded to investigate their penetration into the retina and choroid. Strong fluorescence signals from EPOβ/HA-SH@liposomes, detected using a secondary fluorescent probe (Alexa Fluor 546 goat antirabbit IgG), were observed in both the retina and choroid of mice 3

https://doi.org/10.1021/acs.molpharmaceut.5c00079
Mol. Pharmaceutics 2025, 22, 2287−2305

and 24 h post-treatment in the treated group (Figure 9C). This indicates that EPOβ/HA-SH@liposomes can effectively deliver EPOβ into the retina and choroid, demonstrating their potential for targeted ocular drug delivery.

3.7. Erythropoietin Recovered Mice Visual Functions Against Crushed Retinal Ganglion Cells Axons. After giving mice EPOβ/HA-SH@liposomes eye drops topically five times, we saw a broad and clear fluorescence distribution in the retina 24 h later in the in vivo ocular penetration study in the ocular posterior regions of the mice. This indicates that the liposomal formulation effectively delivered EPOβ into the retinal tissue when applied topically. Conversely, when free EPOβ was applied topically, no significant fluorescence was detected in the retina, as shown in Figure 10A. This suggests that the corneal epithelial cells were unable to uptake free EPOβ effectively via the topical route. The comparison highlights the superior penetration and delivery capabilities of the HA-SH@liposome formulation over free EPOβ, underscoring the potential of these liposomes for enhancing ocular drug delivery and achieving therapeutic concentrations in the retina.

In order to obtain further information, we applied topical EPOβ/HA-SH@liposomes eye drops and then utilized confocal microscopy to look at how much of it penetrated the retina and ganglion cells. The confocal microscopy images confirmed that EPOβ delivered via HA-SH@liposomes successfully penetrated into the retinal layers and ganglion cells (Figure 10B). This detailed visualization provided clear evidence of the effective delivery and localization of EPOβ within the target ocular tissues, reinforcing the potential of this liposomal formulation for targeted ocular drug delivery.

To further confirm our findings, we measured the concentrations of EPOβ in the entire eyeball at various time points following the use of EPOβ/HA-SH@liposome eye drops. This was done using ELISA to quantify the amount of EPOβ and calculate the penetration ratios. The results from the ELISA provided a detailed analysis of how effectively the EPOβ/HA-SH@liposomes penetrated the ocular tissues over time, supporting the observed fluorescence distribution and reinforcing the potential of this liposomal formulation for efficient ocular drug delivery. Excitingly, EPOβ/HA-SH@liposomes demonstrated a high penetration efficiency, approximately 1.9× greater than that of free EPOβ. This significant increase in penetration efficiency highlights the effectiveness of the liposomal formulation in delivering EPOβ into ocular tissues compared to the free form of the protein (Figure 10C).

Most neurodegenerative diseases affecting the retina led to partial or complete irreversible vision loss due to the absence of self-regenerative capabilities and effective treatment options. However, recent strides in cell therapy have sparked hope for promising treatments that could preserve vision in patients afflicted with ocular disorders. RGCs are prone to degeneration and death following direct injuries, like high intraocular pressure or trauma, or from systemic disease-related harmful stimuli. Since visual information is transmitted via RGC axons, the loss of RGCs directly correlates with vision loss.[69]

Even though a number of models have been created to simulate glaucomatous neurodegeneration, they all lead to the loss of retinal ganglion cells as a result of damage to the optic nerve, which is most likely the first insult in glaucomatous disorders. In this way, data on RGC degeneration have been obtained using the optic nerve crush (ONC) model, despite the fact that it does not precisely replicate the pathophysiological pathways of actual glaucoma. To find compounds with therapeutic promise for use as pharmacological treatments against glaucomatous neurodegeneration, the ONC model has been specifically utilized to study the mechanisms behind RGC degeneration.[70]

We used an OptoDrum system to measure the animals' spatial visual acuity 60 days after the injuries. With the help of this method, we were able to precisely gauge the animals' visual capacities, which gave us valuable information about how well the treatment worked over time. The optomotor response, based on head movement and following visual grating stimuli presented on four monitors surrounding the rats, was used to assess visual acuity. We observed that animals treated with EPOβ/HA-SH@liposomes showed a dramatic increase in visual acuity compared to those treated with free EPOβ and HA-SH@liposomes (Figure 10D). Two months post-crush injury, the visual acuity (cycles/degree) in mice treated with EPOβ/HA-SH@liposomes was significantly preserved compared to those treated with free EPOβ (**P = 0.001). These results demonstrate a significant improvement in visual behavior tests following EPOβ/HA-SH@liposomes treatment.

4. CONCLUSIONS

In this study, we developed a novel nanoformulation, EPOβ/HA-SH@liposomes, as a topical eye drop for treating neurodegenerative ocular diseases. Using a post-microfluidic conjugation method, we formulated and applied this liposome-based delivery system to both healthy mice and mice with an ONC model. The optimized formulation (55:25:20 ratio of SPC/DOPE/DOTAP) showed excellent encapsulation efficiency (>90%), which was attributed to strong electrostatic interactions and precise microfluidic encapsulation. This formulation was selected for its superior properties, including a small particle size and PDI. TEM imaging and a shift in the UV−visible spectrum confirmed the successful HA-SH coating on the liposomes. Furthermore, the HA-SH@liposomes stored at 4 °C exhibited excellent physical and chemical stability, with minimal particle size increase during storage. Mucoadhesive studies revealed that HA-SH@liposomes had significantly higher viscosity compared to HA@liposomes and free liposomes, indicating superior mucoadhesive properties, which enhance their effectiveness for ocular drug delivery. In vitro biocompatibility tests on RGC-5 cells showed no significant cytotoxicity for free EPOβ, blank HA-SH@liposomes, or EPOβ/HA-SH@liposomes compared to the control. Fluorescence imaging after administering FITC-labeled HA-SH@liposomes as eyedrops showed strong fluorescence in the corneal epithelium to the endodermis within three hours, indicating effective ocular distribution. After five applications of EPOβ/HA-SH@liposomes, strong fluorescence was observed in the retina 24 h later, while free EPOβ showed no significant fluorescence. ELISA measurements confirmed that EPOβ/HA-SH@liposomes had a penetration efficiency 1.9× higher than free EPOβ, supporting their superior ocular drug delivery capabilities. Optokinetic Response Visual Acuity tests conducted 60 days postinjury using the OptoDrum system demonstrated significantly improved visual acuity in animals treated with EPOβ/HA-SH@liposomes compared to those treated with free EPOβ and HA-SH@liposomes, suggesting improved visual function. Our results indicate that neuroprotective substances such as EPOβ/HA-SH@liposomes can be applied topically to the posterior

https://doi.org/10.1021/acs.molpharmaceut.5c00079
Mol. Pharmaceutics 2025, 22, 2287−2305

part of the eye. This strategy provides a safe, effective, and user-friendly way to maintain visual acuity in both human and animal patients with ischemic or degenerative retinopathies.

■ ASSOCIATED CONTENT

Supporting Information

The Supporting Information is available free of charge at https://pubs.acs.org/doi/10.1021/acs.molpharmaceut.5c00079.

Additional experimental details and characterization data, the synthesis procedure of HA-SH, UV−vis spectra of liposome formulations, drug release kinetic models, fluorescence microscopy images of cellular uptake, in vivo distribution of FITC-labeled HA-SH@liposomes in retinal layers, and table listing antibodies used in the study (PDF)

■ AUTHOR INFORMATION

Corresponding Authors

Mohammad reza Nabid − *Department of Polymer and Materials Chemistry, Faculty of Chemistry & Petroleum Sciences, Shahid Beheshti University, Tehran 1983969411, Iran;* orcid.org/0000-0002-2556-4529; Email: m-nabid@sbu.ac.ir

Hamid Sadeghi Abandansari − *Department of Cell Engineering, Cell Science Research Center, Royan Institute for Stem Cell Biology and Technology, ACECR, Tehran 16635-148, Iran; Department of Stem Cells and Developmental Biology, Faculty of Basic Sciences and Advanced Technologies in Biology, University of Science and Culture, Tehran 1461968151, Iran;* orcid.org/0000-0002-3548-168X; Email: sadeghi.chem89@gmail.com

Authors

Sarvenaz Pakian − *Department of Polymer and Materials Chemistry, Faculty of Chemistry & Petroleum Sciences, Shahid Beheshti University, Tehran 1983969411, Iran*

Leila Satarian − *Department of Brain and Cognitive Sciences, Cell Science Research Center, Royan Institute for Stem Cell Biology and Technology, ACECR, Tehran 16635-148, Iran*

Ahmad Mirkani − *Department of Polymer and Materials Chemistry, Faculty of Chemistry & Petroleum Sciences, Shahid Beheshti University, Tehran 1983969411, Iran*

Complete contact information is available at: https://pubs.acs.org/10.1021/acs.molpharmaceut.5c00079

Funding

No funding to declare.

Notes

The authors declare no competing financial interest.

■ ACKNOWLEDGMENTS

This work was supported by the Shahid Beheshti University Research Council.

■ REFERENCES

(1) Mishra, G. P.; Bagui, M.; Tamboli, V.; Mitra, A. K. Recent applications of liposomes in ophthalmic drug delivery. *J. Drug Deliv.* **2011**, *2011* (1), 863734.

(2) Akhter, M. H.; Ahmad, I.; Alshahrani, M. Y.; Al-Harbi, A. I.; Khalilullah, H.; Afzal, O.; Altamimi, A. S.; Najib Ullah, S. N. M.; Ojha, A.; Karim, S. Drug delivery challenges and current progress in nanocarrier-based ocular therapeutic system. *Gels* **2022**, *8* (2), 82.

(3) Varela-Fernández, R.; Díaz-Tomé, V.; Luaces-Rodríguez, A.; Conde-Penedo, A.; García-Otero, X.; Luzardo-Álvarez, A.; Fernández-Ferreiro, A.; Otero-Espinar, F. J. Drug delivery to the posterior segment of the eye: Biopharmaceutic and pharmacokinetic considerations. *Pharmaceutics* **2020**, *12* (3), 269.

(4) Flaxman, S. R.; Bourne, R. R.; Resnikoff, S.; Ackland, P.; Braithwaite, T.; Cicinelli, M. V.; Das, A.; Jonas, J. B.; Keeffe, J.; Kempen, J. H.; et al. Global causes of blindness and distance vision impairment 1990−2020: a systematic review and meta-analysis. *Lancet Glob. Health* **2017**, *5* (12), e1221−e1234.

(5) Aghdam, K. A.; Sanjari, M. S.; Falavarjani, K. G. Erythropoietin in ophthalmology: a literature review. *J. Curr. Opthamol.* **2016**, *28* (1), 5−11.

(6) Marti, H. H. Erythropoietin and the hypoxic brain. *Journal of Experimental Biology* **2004**, *207* (18), 3233−3242.

(7) Hernández, C.; Fonollosa, A.; García-Ramírez, M.; Higuera, M. n.; Catalán, R.; Miralles, A.; García-Arumí, J.; Simó, R. Erythropoietin is expressed in the human retina and it is highly elevated in the vitreous fluid of patients with diabetic macular edema. *Diabetes care* **2006**, *29* (9), 2028−2033.

(8) GARCia-RAMirez, M.; HERNandez, C.; Simo, R. Expression of erythropoietin and its receptor in the human retina: a comparative study of diabetic and nondiabetic subjects. *Diabetes Care* **2008**, *31* (6), 1189−1194.

(9) Ott, C.; Martens, H.; Hassouna, I.; Oliveira, B.; Erck, C.; Zafeiriou, M.-P.; Peteri, U.-K.; Hesse, D.; Gerhart, S.; Altas, B.; et al. Widespread expression of erythropoietin receptor in brain and its induction by injury. *Molecular medicine* **2015**, *21*, 803−815.

(10) Luo, W.; Hu, L.; Wang, F. The protective effect of erythropoietin on the retina. *Ophthalmic research* **2015**, *53* (2), 74−81.

(11) Resende, A. P.; São-Braz, B.; Delgado, E. Alternative route for erythropoietin ocular administration. *Graefes Arch. Clin. Exp. Opthalmol.* **2013**, *251*, 2051−2056.

(12) Resende, A. P.; São Braz, B.; Delgado, E. Ocular erythropoietin penetration after subconjunctival administration in glaucomatous rats. *Ophthalmic Research* **2016**, *56* (2), 104−110.

(13) Resende, A. P.; Rosolen, S. G.; Nunes, T.; São Braz, B.; Delgado, E. Functional and structural effects of erythropoietin subconjunctival administration in glaucomatous animals. *Biomedicine hub* **2018**, *3* (2), 1−11.

(14) Bartesaghi, S.; Marinovich, M.; Corsini, E.; Galli, C. L.; Viviani, B. Erythropoietin: a novel neuroprotective cytokine. *Neurotoxicology* **2005**, *26* (5), 923−928.

(15) Bond, W. S.; Rex, T. S. Evidence that erythropoietin modulates neuroinflammation through differential action on neurons, astrocytes, and microglia. *Front. Immunol.* **2014**, *5*, 523.

(16) Tsai, J. C.; Wu, L.; Worgul, B.; Forbes, M.; Cao, J. Intravitreal administration of erythropoietin and preservation of retinal ganglion cells in an experimental rat model of glaucoma. *Current Eye Research* **2005**, *30* (11), 1025−1031.

(17) Zhong, Y.-s.; Liu, X.-h.; Cheng, Y.; Min, Y.-j. Erythropoietin with retrobulbar administration protects retinal ganglion cells from acute elevated intraocular pressure in rats. *Journal of ocular pharmacology and therapeutics* **2008**, *24* (5), 453−460.

(18) da Silva, B. R. F. D. Retinal Erythropoietin Distribution and Neuroprotective Effect in a Nanoparticulate Drug Delivery System After Subconjunctival and Topical Administration in an Animal Glaucoma Model. Doctoral Thesis, Universidade de Lisboa, Lisbon, Portugal, 2023.

(19) Ranta, V.-P.; Urtti, A. Transscleral drug delivery to the posterior eye: prospects of pharmacokinetic modeling. *Advanced drug delivery reviews* **2006**, *58* (11), 1164−1181.

(20) Rodrigues, G. A.; Lutz, D.; Shen, J.; Yuan, X.; Shen, H.; Cunningham, J.; Rivers, H. M. Topical drug delivery to the posterior segment of the eye: addressing the challenge of preclinical to clinical translation. *Pharm. Res.* **2018**, *35* (12), 245.

(21) Xie, G.; Lin, S.; Wu, F.; Liu, J. Nanomaterial-based ophthalmic drug delivery. *Adv. Drug Delivery Rev.* **2023**, *200*, 115004.
(22) Kumar, M.; Tiwari, A.; Asdaq, S. M. B.; Nair, A. B.; Bhatt, S.; Shinu, P.; Al Mouslem, A. K.; Jacob, S.; Alamri, A. S.; Alsanie, W. F.; et al. Itraconazole loaded nano-structured lipid carrier for topical ocular delivery: Optimization and evaluation. *Saudi J. Biol. Sci.* **2022**, *29* (1), 1−10.
(23) Laradji, A.; Karakocak, B. B.; Kolesnikov, A. V.; Kefalov, V. J.; Ravi, N. Hyaluronic acid-based gold nanoparticles for the topical delivery of therapeutics to the retina and the retinal pigment epithelium. *Polymers* **2021**, *13* (19), 3324.
(24) Resende, A. P.; Silva, B.; Braz, B. S.; Nunes, T.; Gonçalves, L.; Delgado, E. Ex vivo permeation of erythropoietin through porcine conjunctiva, cornea, and sclera. *Drug delivery and translational research* **2017**, *7*, 625−631.
(25) Wang, Y.; Xu, X.; Gu, Y.; Cheng, Y.; Cao, F. Recent advance of nanoparticle-based topical drug delivery to the posterior segment of the eye. *Expert opinion on drug delivery* **2018**, *15* (7), 687−701.
(26) Kaur, I. P.; Kakkar, S. Nanotherapy for posterior eye diseases. *J. Controlled Release* **2014**, *193*, 100−112.
(27) Weng, Y.; Liu, J.; Jin, S.; Guo, W.; Liang, X.; Hu, Z. Nanotechnology-based strategies for treatment of ocular disease. *Acta pharmaceutica sinica B* **2017**, *7* (3), 281−291.
(28) Ameeduzzafar; Ali, J.; Fazil, M.; Qumbar, M.; Khan, N.; Ali, A. Colloidal drug delivery system: amplify the ocular delivery. *Drug delivery* **2016**, *23* (3), 700−716.
(29) Silva, B.; Gonçalves, L. M.; Braz, B. S.; Delgado, E. Chitosan and hyaluronic acid nanoparticles as vehicles of epoetin beta for subconjunctival ocular delivery. *Marine Drugs* **2022**, *20* (2), 151.
(30) Silva, B.; Gonçalves, L. M.; São Braz, B.; Delgado, E. Topical ocular delivery of nanoparticles with epoetin beta in Wistar Hannover rats. *Sci. Rep.* **2023**, *13*, 1559.
(31) Yavuz, B.; Kompella, U. B. Ocular drug delivery. *Pharmacologic Therapy of Ocular Disease* **2016**, *242*, 57−93.
(32) Taylor, K. M.; Aulton, M. E. *Aulton's pharmaceutics E-Book: The design and manufacture of medicines*, 6th ed.; Elsevier Health Sciences, 2021.
(33) Tasharrofi, N.; Nourozi, M.; Marzban, A. How liposomes pave the way for ocular drug delivery after topical administration. *Journal of Drug Delivery Science and Technology* **2022**, *67*, 103045.
(34) Schaeffer, H. E.; Krohn, D. L. Liposomes in topical drug delivery. *Invest. Ophthalmol. Vis. Sci.* **1982**, *22* (2), 220−227.
(35) Ludwig, A. The use of mucoadhesive polymers in ocular drug delivery. *Advanced drug delivery reviews* **2005**, *57* (11), 1595−1639.
(36) Bian, S.; He, M.; Sui, J.; Cai, H.; Sun, Y.; Liang, J.; Fan, Y.; Zhang, X. The self-crosslinking smart hyaluronic acid hydrogels as injectable three-dimensional scaffolds for cells culture. *Colloids and Surfaces B: Biointerfaces* **2016**, *140*, 392−402.
(37) Jeon, S.; Yoo, C. Y.; Park, S. N. Improved stability and skin permeability of sodium hyaluronate-chitosan multilayered liposomes by Layer-by-Layer electrostatic deposition for quercetin delivery. *Colloids and surfaces B: biointerfaces* **2015**, *129*, 7−14.
(38) Apaolaza, P.; Busch, M.; Asin-Prieto, E.; Peynshaert, K.; Rathod, R.; Remaut, K.; Dünker, N.; Göpferich, A. Hyaluronic acid coating of gold nanoparticles for intraocular drug delivery: Evaluation of the surface properties and effect on their distribution. *Experimental eye research* **2020**, *198*, 108151.
(39) Tsakiri, M.; Tabriz, A. G.; Naziris, N.; Rahali, K.; Douroumis, D.; Demetzos, C. Exosome-like genistein-loaded nanoparticles developed by thin-film hydration and 3D-printed Tesla microfluidic chip: A comparative study. *Int. J. Pharm.* **2024**, *651*, 123788.
(40) Cong, W.; Liu, Q.; Chen, X.; Gao, R.; Lu, J.; Wang, Y.; Luo, G. Characterization and pharmacokinetics of a novel pirarubicin liposome powder. *Drug development and industrial pharmacy* **2010**, *36* (10), 1186−1194.
(41) Katharotiya, K.; Shinde, G.; Katharotiya, D.; Shelke, S.; Patel, R.; Kulkarni, D.; Panzade, P. Development, evaluation and biodistribution of stealth liposomes of 5-fluorouracil for effective treatment of breast cancer. *Journal of Liposome Research* **2022**, *32* (2), 146−158.
(42) Shastri, D. H.; Patel, L.; Parikh, R. Studies on in situ hydrogel: a smart way for safe and sustained ocular drug delivery. *Journal of Young Pharmacists* **2010**, *2* (2), 116−120.
(43) Salzillo, R.; Schiraldi, C.; Corsuto, L.; D'Agostino, A.; Filosa, R.; De Rosa, M.; La Gatta, A. Optimization of hyaluronan-based eye drop formulations. *Carbohydrate polymers* **2016**, *153*, 275−283.
(44) Kamiloglu, S.; Sari, G.; Ozdal, T.; Capanoglu, E. Guidelines for cell viability assays. *Food frontiers* **2020**, *1* (3), 332−349.
(45) Eghbali, A.; Anvarinia, Y.; Sanjari, M. S.; Pakdel, F.; Seyedsadr, M.; Mazinani, F. H.; Zare, L.; Zarei-Kheirabadi, M.; Satarian, L. Erythropoietin protects against retinal damage in A rat model of optic neuropathy via glial suppression. *Cell J.* **2023**, *25* (5), 327.
(46) Butterworth, P.; Baum, H.; Porter, J. A modification of the Ellman procedure for the estimation of protein sulfhydryl groups. *Arch. Biochem. Biophys.* **1967**, *118* (3), 716−723.
(47) Pakian, S.; Mirkani, A.; Sadeghi-Abandansari, H.; Nabid, M.-R. Stabilization of Cationic Liposomes Using Hyaluronic acid-modified Gold Nanoparticles by Post-Microfluidics Conjugation Approach for Drug Delivery Applications. *Journal of Drug Delivery Science and Technology* **2024**, *99*, 105956.
(48) Weaver, E.; Mathew, E.; Caldwell, J.; Hooker, A.; Uddin, S.; Lamprou, D. A. The manufacturing of 3D-printed microfluidic chips to analyse the effect upon particle size during the synthesis of lipid nanoparticles. *Journal of Pharmacy and Pharmacology* **2023**, *75* (2), 245−252.
(49) Jaradat, E.; Weaver, E.; Meziane, A.; Lamprou, D. A. Synthesis and Characterization of Paclitaxel-Loaded PEGylated Liposomes by the Microfluidics Method. *Molecular Pharmaceutics* **2023**, *20* (12), 6184−6196.
(50) Campbell, R. B.; Balasubramanian, S. V.; Straubinger, R. M. Phospholipid-cationic lipid interactions: influences on membrane and vesicle properties. *Biochimica et Biophysica Acta (BBA)-Biomembranes* **2001**, *1512* (1), 27−39.
(51) Park, H.; Lee, S.-H.; Ahn, J. C.; Rajendiran, J. C. B.; Arai, Y. Influence of cationic lipid concentration on properties of lipid-polymer hybrid nanospheres for gene delivery. *Int. J. Nanomed.* **2015**, 5367−5382.
(52) Zhang, Y.; Anchordoquy, T. J. The role of lipid charge density in the serum stability of cationic lipid/DNA complexes. *Biochimica et Biophysica Acta (BBA)-Biomembranes* **2004**, *1663* (1−2), 143−157.
(53) Jain, A. K.; Thareja, S. In vitro and in vivo characterization of pharmaceutical nanocarriers used for drug delivery. *Artificial cells, nanomedicine, and biotechnology* **2019**, *47* (1), 524−539.
(54) Lee, C.-Y.; Wang, W.-T.; Liu, C.-C.; Fu, L.-M. Passive mixers in microfluidic systems: A review. *Chemical Engineering Journal* **2016**, *288*, 146−160.
(55) Wang, L.; Wang, N.; Zhang, W.; Cheng, X.; Yan, Z.; Shao, G.; Wang, X.; Wang, R.; Fu, C. Therapeutic peptides: current applications and future directions. *Sig. Transduct. Target Ther.* **2022**, *7*, 48.
(56) Torchilin, V. P. Recent advances with liposomes as pharmaceutical carriers. *Nature reviews Drug discovery* **2005**, *4* (2), 145−160.
(57) Szoka, F., Jr; Papahadjopoulos, D. Comparative properties and methods of preparation of lipid vesicles (liposomes). *Annual review of biophysics and bioengineering* **1980**, *9* (1), 467−508.
(58) Gelzleichter, T. R. Early characterization of biosimilar therapeutics. In *Nonclinical development of novel biologics, biosimilars, vaccines and specialty biologics*, Elsevier, 2013; pp 185−210.
(59) Vedadghavami, A.; Zhang, C.; Bajpayee, A. G. Overcoming negatively charged tissue barriers: Drug delivery using cationic peptides and proteins. *Nano today* **2020**, *34*, 100898.
(60) García-Posadas, L.; Contreras-Ruiz, L.; López-García, A.; Villarón Álvarez, S.; Maldonado, M. J.; Diebold, Y. Hyaluronan receptors in the human ocular surface: a descriptive and comparative study of RHAMM and CD44 in tissues, cell lines and freshly collected samples. *Histochemistry and cell biology* **2012**, *137*, 165−176.

https://doi.org/10.1021/acs.molpharmaceut.5c00079
Mol. Pharmaceutics 2025, 22, 2287−2305

(61) Yang, X.-y.; Li, Y.-x.; Li, M.; Zhang, L.; Feng, L.-x.; Zhang, N. Hyaluronic acid-coated nanostructured lipid carriers for targeting paclitaxel to cancer. *Cancer letters* **2013**, *334* (2), 338−345.
(62) Tiantian, Y.; Wenji, Z.; Mingshuang, S.; Rui, Y.; Shuangshuang, S.; Yuling, M.; Jianhua, Y.; Xinggang, Y.; Shujun, W.; Weisan, P. Study on intralymphatic-targeted hyaluronic acid-modified nanoliposome: Influence of formulation factors on the lymphatic targeting. *Int. J. Pharm.* **2014**, *471* (1−2), 245−257.
(63) Ripoll, M.; Martin, E.; Enot, M.; Robbe, O.; Rapisarda, C.; Nicolai, M.-C.; Deliot, A.; Tabeling, P.; Authelin, J.-R.; Nakach, M.; et al. Optimal self-assembly of lipid nanoparticles (LNP) in a ring micromixer. *Sci. Rep.* **2022**, *12*, 9483.
(64) Guldiken, B.; Gibis, M.; Boyacioglu, D.; Capanoglu, E.; Weiss, J. Physical and chemical stability of anthocyanin-rich black carrot extract-loaded liposomes during storage. *Food research international* **2018**, *108*, 491−497.
(65) Jyothi, V. G. S.; Bulusu, R.; Rao, B. V. K.; Pranothi, M.; Banda, S.; Bolla, P. K.; Kommineni, N. Stability characterization for pharmaceutical liposome product development with focus on regulatory considerations: An update. *Int. J. Pharm.* **2022**, *624*, 122022.
(66) Felgner, P. L.; Gadek, T. R.; Holm, M.; Roman, R.; Chan, H. W.; Wenz, M.; Northrop, J. P.; Ringold, G. M.; Danielsen, M. Lipofection: a highly efficient, lipid-mediated DNA-transfection procedure. *Proceedings of the National Academy of Sciences* **1987**, *84* (21), 7413−7417.
(67) Junk, A. K.; Mammis, A.; Savitz, S. I.; Singh, M.; Roth, S.; Malhotra, S.; Rosenbaum, P. S.; Cerami, A.; Brines, M.; Rosenbaum, D. M. Erythropoietin administration protects retinal neurons from acute ischemia-reperfusion injury. *Proceedings of the National Academy of Sciences* **2002**, *99* (16), 10659−10664.
(68) Feizi, S.; Alemzadeh-Ansari, M.; Karimian, F.; Esfandiari, H. Use of erythropoietin in ophthalmology: A review. *Survey of Ophthalmology* **2022**, *67* (2), 427−439.
(69) Almasieh, M.; Wilson, A. M.; Morquette, B.; Vargas, J. L. C.; Di Polo, A. The molecular basis of retinal ganglion cell death in glaucoma. *Prog. Retinal Eye Res.* **2012**, *31* (2), 152−181.
(70) Cammalleri, M. Optic nerve crush as a model of retinal ganglion cell degeneration. *Annals of Eye Science* **2022**, *7*, 17−17.

https://doi.org/10.1021/acs.molpharmaceut.5c00079
Mol. Pharmaceutics 2025, 22, 2287−2305